Dysbindin-1 Isoform-Specific Modulation of Astrocytic and Basal Ganglia Dopamine/Behavioral Phenotypes

Rosa Mastrogiacomo[1#], Gabriella Trigilio[1,2#], Céline Devroye[1], Daniel Dautan[1,3], Valentina Ferretti[1], Gabriele Losi[4,5], Lucia Caffino[6], Genny Orso[7], Roberto Marotta[1], Federica Maltese[1], Gessica Piras[8], Alessia Forgiarini[7], Giada Pacinelli[1], Annamaria Lia[4,5], Debora A. Rothmond[9], John L. Waddington[10], Filippo Drago[2], Fabio Fumagalli[6], Maria Antonietta De Luca[8], Gian Marco Leggio[2], Giorgio Carmignoto[4,5], Cynthia S. Weickert[9], Francesca Managò[1†], Francesco Papaleo[1,3†*].

[1]*Genetics of Cognition laboratory, Neuroscience area, Istituto Italiano di Tecnologia, via Morego, 30, 16163 Genova, Italy.*
[2]*Department of Biomedical and Biotechnological Sciences, University of Catania, Catania, Italy.*
[3]*Fondazione IRCCS Ca' Granda Ospedale Maggiore Policlinico, Milano, Italy.*
[4]*Neuroscience Institute, CNR, Padova, Italy.*
[5]*Department of Biomedical Science, University of Padova, Italy.*
[6]*Department of Pharmacological and Biomolecular Sciences, Università degli Studi di Milano, Milan, Italy.*
[7]*Department of Pharmaceutical and Pharmacological Sciences, University of Padova, Padova, Italy.*
[8]*Department of Biomedical Sciences, University of Cagliari, Cagliari, Italy.*
[9]*Schizophrenia Research Laboratory, Neuroscience Research Australia, Sydney, Australia.*
[10]*School of Pharmacy and Biomolecular Sciences, Royal College of Surgeons in Ireland, Dublin 2, Ireland.*

[#]equal contribution

[†]co-senior authors

[*]Correspondence: francesco.papaleo@iit.it

Abstract

Background. The mechanisms underlying the dichotomic cortical/basal ganglia dopaminergic abnormalities in schizophrenia are unclear. Astrocytes are important non-neuronal modulators of brain circuits, but their role in dopaminergic system remains poorly explored.

Methods. Microarray analyses, immunohistochemistry, and two-photon laser scanning microscopy were used to delineate the impact of dysbindin-1 (Dys1) on astrocytic reactivity. *In vitro* cell cultures and gene expression analyses from post-mortem human and mouse brains were used to explore distinct neuronal/astrocytes expression and developmental patterns of Dys1 isoforms. A comprehensive behavioral and electrochemical assessment in mice selectively lacking the Dys1A isoform unraveled then Dys1 isoform-specific impact on cortical/basal ganglia dopaminergic and behavioral phenotypes. *Ex vivo* electron microscopy and protein expression analyses corroborated the isoform-specific Dys1 influence in distinct neuronal/astrocytic intracellular trafficking processes. Finally, post-mortem human samples from healthy subjects and schizophrenia cases were used to explore the clinical relevance of basal ganglia Dys1 isoform-specific processes.

Results. Dys1 hypofunction increases the reactivity of astrocytes, which express only the Dys1A isoform. Notably, selective Dys1A disruption results in behavioral and dopaminergic/D2 alterations ascribable to functioning in basal ganglia, but not in the cortex. Moreover, selective Dys1A disruption alters intracellular trafficking in astrocytes, but not in neurons. These processes have clinical relevance because the caudate and not the cortex of patients with schizophrenia shows a selective reduction of the Dys1A isoform.

Conclusions. We show a hitherto unknown role for the Dys1A isoform in the astrocytic machinery associated with selective alterations of basal ganglia behavioral and dopaminergic phenotypes relevant to schizophrenia.

Keywords

51 Astrocytes; dopamine; dysbindin-1A; D2 receptor; schizophrenia; globus pallidus external segment;
52 motivation; sensorimotor gating.
53

Introduction

Dysbindin-1 (Dys1) protein, coded by the Dystrobrevin Binding Protein 1 (DTNBP1) gene, has been implicated in cognitive processes (1, 2), responses to antipsychotic drugs (1, 3, 4), and genetic risk for schizophrenia (3-5). In agreement, dystrophin and its binding partners (Dys1 being a component of the dystrophin complex) are implicated in schizophrenia (6), in line with linkage studies (7-10), and evidence of reduced Dys1 levels in post-mortem brain samples from patients with schizophrenia (11, 12). These clinical implications have been linked to Dys1-related modulation of neuronal dopaminergic and glutamatergic signaling (3, 4, 12-15), through receptor-mediated intracellular trafficking mechanisms, including D2-like receptors (1, 3, 16, 17).

Drosophila dysbindin (dDys) has shown dichotomic regulation of glutamatergic and dopaminergic transmission, with the latter involving glial cells (18). Notably, an active role for astrocytes in dopaminergic signaling has emerged (19-22). However, whether Dys1 might participate in the machinery of astrocytic activity and related control of dopaminergic signaling is unexplored. Similarly, the behavioral implications and possible clinical relevance of astrocytic regulation remain unknown. In mammals, Dys1 exists in at least three spliced transcripts, Dys1A, 1B, and 1C (17), with 1A and 1C being orthologues in humans and mice (14, 17, 23). These isoforms are believed to have distinct functions as they are differentially distributed in brain synaptosomes, are present in different functional domains, and have distinct binding partners (14, 24, 25). However, the contribution of each Dys1 isoform in physiological functions, specifically in astrocyte activity, and the related behavioral outcomes, is unknown.

Here, we report that the Dys1A spliced transcript is prevalently implicated in astrocytic machinery, as well as in basal ganglia dopamine/D2 signaling and related behavioral processes. We show that clinically relevant Dys1 genetic variations alter astrocyte activity. Specifically, we find that Dys1A is the only isoform expressed in astrocytes and is preferentially involved in astrocytic, but not neuronal, intracellular trafficking. Notably, selective disruption of Dys1A induces behavioral and dopaminergic alterations related to the basal ganglia, while sparing them at the cortical level. This might

be clinically relevant as we found that, in contrast to data from cortical samples, Dys1A is decreased in the caudate of patients with schizophrenia. Overall, we show a hitherto unknown role for Dys1A-astrocyte-dopamine interaction in the basal ganglia mediating behavioral dysfunctions relevant to schizophrenia.

Methods and Materials

Mice

All procedures were approved by the Italian Ministry of Health (permit n. 230/2009-B, 107/2015-PR, and 749/2017-PR) and local Animal Use Committee and were conducted in accordance with the Guide for the Care and Use of Laboratory Animals of the National Institutes of Health and European Community Council Directives. Routine veterinary care and animal maintenance were provided by dedicated and trained personnel. Male and female littermate mice between 3-7 months of age were used. Animals were housed 2-4 per cage, in a climate-controlled animal facility (22°C ± 2°C) and maintained on a 12-hr light/dark cycle (08:00 on; 20:00 off), with food and water available *ad libitum.* The experimenter handled the mice on alternate days during the week preceding the tests. Body weight and general appearance of mice were recorded before starting behavioral testing.

Dys1 and Dys1A mutant mice. The Dys1 heterozygous mutant mice (Dys1+/−) and their wild-type littermates (Dys1+/+), on C57BL6/J background were bred and used as previously described (1, 3). The $Dys1A_{flox/flox}$ mice generated by Glaxo SmithKline (26) were retained on C57BL6/J background and presented two loxP sites flanking exon 5, which is necessary for correct expression of the Dys1A long isoform. Constitutive Dys1A deletion (Dys1A-/-) or partial reduction (Dys1A+/-) was obtained crossing $Dys1A_{flox/flox}$ mice with a germline Cre deleter transgenic strain (Taconic-Artemis Germany). The breeding scheme used consisted of mating one male Dys1A+/- with two Dys1A+/- females. All mutant mice used were viable, fertile, normal in size and did not display any gross physical or behavioral abnormalities.

Behavior

Locomotor activity. Mice were tested in an experimental apparatus consisting of four gray, opaque open field boxes (40x40x40 cm) evenly illuminated by overhead lighting (5±1 lux). Each session was video-recorded using an overhead camera from ANY-maze (Stoelting Co., Wood Dale, IL, USA)

with the experimenter absent from the room during the test. Activity was tracked during the first exposure to the empty open field arena for 30 minutes. For amphetamine experiments, mice were tested in the same open field arenas. First, mice were placed in the empty open field and allowed to explore for 10 minutes. Then, mice were removed from the arena, injected with 1.5 mg/kg/10ml D-amphetamine sulphate (i.p.; Sigma-Aldrich) and returned to the open field for an additional 60 minutes. This procedure was repeated for five consecutive days. All sessions were videotaped and tracked with ANY-maze software (Stoelting Co.).

Male-female social interaction. The test was conducted in Tecniplast cages (35x23x19 cm) illuminated (5±1 lux) and video-recorded using a Unibrain Fire-i digital camera. The video camera was mounted facing the front of the cage to record the session for subsequent scoring of social investigation parameters as previously described (27). Unfamiliar female stimulus mice in estrus were matched to the subject male mice by age and maintained in social groups of four per home cage.

Social habituation/dishabituation task. Naıve mice were tested in Tecniplast cages (35x23x19 cm) illuminated (5±1 lux) and video-recorded using a Unibrain Fire-i digital camera. As described previously (27), mice were placed individually for environmental habituation to the test cage 1h prior to testing. A stimulus mouse (unfamiliar of the same sex) was introduced into the testing cage for a 1-min interaction. At the end of the 1-min trial, the stimulus animal was removed and returned to an individual holding cage for 3 minutes. We repeated this sequence for three trials with 3-min inter-trial intervals. In a fifth 'dishabituation' trial, we introduced a new (unfamiliar) stimulus mouse into the testing cage. Videos of behaviors were recorded and subsequently scored offline.

Attentional set-shifting task. Attentional set-shifting was tested in the two-chamber intradimensional/extradimensional (ID/ED) Operon task as previously described (3, 28). After random selection of mice for the ID/ED task, all behavioral parameters were obtained blind to the genotype of the animals. For habituation to the apparatus, during the first 2 days mice were habituated for 45 min to the apparatus with only neutral stimuli (Habituation 1) and trained to move from one chamber to the other (Habituation 2). Any nose poke into the nose-poke holes resulted in a pellet delivery into the

food receptacle. The next day, mice were trained to perform two randomly presented simple discriminations (e.g. between smooth vs. sand cardboard; light on vs. light off; peach vs. sage) so that they were familiar with the stimulus dimensions (Habituation 3). These exemplars were not used again. The mice had to reach a criterion of eight correct choices out of ten consecutive trials to complete this and each following testing stage. Performance was measured in all phases of all experiments using number of trials to reach the criterion; time (in minutes) to reach the criterion and time (in seconds) from breaking the photobeams adjacent to the automated door to a nose-poke response (latency to respond). A session started when a mouse was placed in one of the two chambers where all the stimuli were neutral. Then the transparent door was dropped to give the mouse access to the other chamber where the stimuli cues were on. The series of stages comprised a simple discrimination (SD), compound discrimination (CD), compound discrimination reversal (CDRe), intradimensional shift (IDS), IDS reversal (IDSRe), a second IDS (IDS2), IDS2 reversal (IDS2Re), extradimensional shift (EDS), and EDS reversal (EDSRe). The mice were exposed to the tasks in this order so that they could develop a set, or bias, toward discriminating between the correct and incorrect nose poke hole.

Acoustic startle response and prepulse inhibition (PPI). Acoustic startle response and PPI were measured using SR-Lab Systems (San Diego Instruments, San Diego, CA, USA) and TSE Startle Response System (TSE Systems GmbH, Bad Homburg, Germany) following previously described protocols (1, 29). Briefly, a sudden acoustic stimulus (120 dB) elicits the startle response, while an acoustic, non-startling pre-pulse (74; 78; 82; 86; 90 dB) preceding the startle stimulus inhibits the startle response (PPI). The startle response elicited by sudden sensory stimuli and its PPI are among some of the most widely studied phenotypes that are highly conserved across mammalian species. A background level of 70 dB white noise was maintained throughout the test session.

Progressive ratio test. We tested mice in a motivational nose-poke operant paradigm for 14 mg 5-TUL pellets (Test Diet) as described previously (30). To avoid confounding factors linked to food restriction/deprivation experience, mice were always provided with food and water *ad libitum*. The operant chambers used (MED Associates Inc, VT, USA) were equipped with two nose-poke holes

mounted at the left and right of a central food magazine, each equipped with infrared photobeams connected to a computer with MED-PC V software. Nose poking into one of the two holes resulted in pellet delivery (active hole), whereas nose poking into the other hole (inactive hole) triggered the house light for 5 seconds (left and right randomly assigned and balanced between groups). Free water was available all times via a water bottle dispenser. Pellets were delivered to the food magazine by an automated dispenser situated outside the experimental chamber. Mice were placed into the operant chambers in the evening around 17:00 and taken out the following morning around 9:00-10:00. Lights within the sound attenuating boxes in which the operant chambers were located ensured mice experienced a light/dark cycle identical to that of holding rooms. Training and testing started automatically from the beginning to the end of the dark phase (20:00 to 8:00). Initially, a fixed ratio (FR)-1 reinforcement schedule was applied, i.e. one nose poke in the active hole resulted in delivery of one pellet. Mice were exposed to the FR1 schedule until they reached the criterion of > 80% active pokes during the entire night for two consecutive nights. Mice that met this learning criterion were switched to a FR3 reinforcement schedule, i.e. three nose-pokes in the active hole produced delivery of one pellet. The FR3 reinforcement schedule lasted two nights if mice met the criterion of > 80% active pokes during the entire night. Afterward, mice were exposed to a progressive ratio (PR) schedule that lasted two hours from the beginning of the night phase and was changed nightly; first night: PR3; second night: PR6; and third night: PR9. Mice were returned to their home cage after the PR test. During the PR experiment, the number of active nose-pokes required to obtain each successive food pellet was progressively increased by three (PR3, 3n+3), six (PR6, 6n+6) and 9 (PR9, 9n+9; where n=number of pellets earned). For example, in PR3 earning the first reinforcer required three active nose pokes, the second six nose pokes, the third nine nose pokes, etc. Likewise, in PR9 earning the first reinforcer required 9 active nose-pokes, the second eighteen nose-pokes, the third twenty-seven nose-pokes, etc. Following each PR session, we calculated the breakpoint (BP) as the last ratio level completed before the end of the two-hour testing session. For example, under the PR3 or the PR9 reinforcement schedules, to earn the third food pellet a mouse had to poke 3+6+9 or 9+18+27 times in the active hole, and thus was given a BP value of 9

or 27, respectively. The BP is a well-validated measure reflecting the strength of the reinforcer and the motivational state of the animal (30).

Immunohistochemistry

Mice were deeply anesthetized (urethane 20%) and perfused transcardially with PBS followed by 4% formaldehyde solution (Sigma-Aldrich) in PBS, pH 7.4. Brains were extracted, post fixed overnight in 4% formaldehyde and cryoprotected in 30% sucrose in PBS. 40-µm-thick coronal sections containing regions of interest were cut on a freezing microtome (VT1000S, Leica Camera AG, Wetzlar, Germany) and collected in PBS before being processed for immunohistochemistry. For GFAP immunostaining, free-floating slices were first washed once in 0.3% Triton X-100 PBS (PBS-T) for 10 minutes, and twice with 0.1% PBS-T, then incubated for 1 h in a blocking solution of 5% normal goat serum (NGS) in 0.1 % PBS-T. Subsequently they were incubated overnight at 4 °C with 1:300 rabbit polyclonal anti-GFAP antibody (Novus Biologicals, Centennial, CO, USA) in blocking solution. Slices were then mounted with ProLong™ Gold Antifade Mountant (ThermoFisher Scientific) and imaged in an inverted laser scanning confocal microscope (A1 Nikon, Shinjuku, Japan) using a 20x or 40x objective. Quantification and analysis were performed using Fiji software (Wayne Rasband, NIH, USA), outlining regions of interest.

Electron microscopy

Mouse brains were perfused with 4% formaldehyde and 2% glutaraldehyde and embedded as described previously (31). Bright field transmission electron microscopy images were acquired from thin (70 nm) sections using a Gatan Orius SC1000 series CCD camera (4008 x 2672 active pixels) (Gatan, Pleasanton, USA), fiber optically coupled to high-resolution phosphor scintillator under a JEOL JEM-1011 transmission electron microscope (TEM) (JEOL, Tokyo, Japan) with thermionic source (W filament) and maximum acceleration voltage 100 kV. All transverse sections of the Golgi

Complex (GC) were taken at the same magnification (x6000) and analyzed using point-counting procedures, with surface densities of Golgi Complex (Sv_iGC) and Cytoplasm (Sv_iCYT) determined according to Leitz ASM system. Moreover, a qualitative score from 1 to 3 was assigned by two different persons blind to the experimental groups to all GC: the maximum score (3) was given when finding a group of cisternae organized in stacks containing tubular and vesicular structures, as defined for GC, and the lower score (1) was given when GC structure was destroyed. Double tilt high angular annular dark field (HAADF) scanning TEM (STEM) tomography was performed using a Tecnai F20 transmission electron microscope (FEI Company, Eindhoven, The Netherlands), equipped with a field-emission gun operating at 200 kV and a Gatan Ultrascan US1000 (Gatan, Pleasanton, USA). For reconstruction of the Golgi apparatus in Dys1+/- mouse astrocytes a 300-nm-thick section was tilted through ±60° with the following tilt scheme: 1° at tilt higher than ±30° and 2° intervals at intermediate tilts. The images were acquired using a HAADF detector at a magnification of x40,000. Computation of each double tilt tomogram was performed by combining two tilt series taken around two orthogonal axes with the IMOD software package. 3D reconstruction was performed using Amira™ Software (Thermo Fisher Scientific).

Cell cultures

Astrocyte-enriched cell cultures were obtained from cortices dissected from post natal day 1 (PND1) mice. Pups were sacrificed by cervical dislocation and cortices were quickly dissected in ice-cold HBSS (Hanks' Balanced Salt Solution, Gibco ThermoFisher Scientific). Samples were incubated in HBSS with 0.125% Trypsin-EDTA (ThermoFisher Scientific) and 1 mg/mL DNAase I (Sigma-Aldrich) for 20 minutes at 37°C. A solution of DMEM (Dulbecco's Modified Eagle Medium, Gibco ThermoFisher Scientific) with 10% horse serum and 1% Penicillin-Streptomycin (Sigma-Aldrich) was added to the samples, which were then centrifuged at 1200 rpm and washed twice in complete medium. Samples were dissociated mechanically in complete medium and filtered through 40 μm cell strainers. Cell suspensions were finally plated on poly-D-lysine coated plates. Cells were cultured

until 100% confluence. Neuronal cell cultures were obtained from E18 mice embryos. Cortices were dissected in ice-cold HBSS and incubated in HBSS with 0.125% Trypsin-EDTA and 0,25 mg/mL DNAase I for 30 minutes at 37°C. A solution of Neurobasal™ medium (Gibco ThermoFisher Scientific) with 10% inactivated fetal bovine serum (Sigma-Aldrich), 1% penicillin-streptomycin, 1% GlutaMAX™ Supplement and 2% B27™ Supplement (Gibco ThermoFisher Scientific) was added to the samples, which were then centrifuged 1200 rpm and resuspended in complete medium before mechanical dissociation. Samples were filtered with 40 μm cell strainers, centrifuged 700 rpm and resuspended in complete medium. Cell suspensions were finally plated on poly-D-lysine coated plates. Neurons were cultured until complete maturation.

Western Blot

For western blot analysis of Dys1 isoforms, we used Dys1+/+ mice at embryonic stage E14.5, PND7, PND35 and PND90, Dys1 and Dys1A knockout mice, glial and neuronal cell cultures. Animals were sacrificed by cervical dislocation; brains were rapidly dissected and stored at -80°. Tissues or cultured cells were lysed in RIPA buffer and Protease Inhibitor Cocktail (Sigma-Aldrich). Western blot analysis was performed using mouse polyclonal anti-dysbindin antibody (PA3111 validated and produced by (17) and anti-actin antibody (Sigma Aldrich). Protein (25μg) from precipitated homogenates was separated on SDS-PAGE, electro- transferred onto nitrocellulose membranes, and then probed with primary antibodies: mouse monoclonal anti-dysbindin antibody (1:1000) and mouse anti-actin antibody (1:10000). Immune complexes were detected using appropriate peroxidase-conjugated secondary antibodies (Thermo Fisher Scientific) and a chemiluminescent reagent (ECL prime; GE Healthcare Europe GmbH, Milan, Italy). Densitometric analysis was performed using ImageQuantTL software (GE Healthcare Europe GmbH). Results were normalized to respective control conditions. For western blot analyses in globus pallidus externus (GPe), GPe were homogenized in a glass–glass potter in cold 0.32-M sucrose buffer pH 7.4 containing 1-mM HEPES, 0.1-mM PMSF, in presence of commercial cocktails of protease (Roche, Monza, Italy) and phosphatase (Sigma-Aldrich, Milan,

Italy) inhibitors and then sonicated. Total proteins have been measured in the total homogenate according to the Bradford Protein Assay procedure (Bio-Rad, Milan, Italy), using bovine serum albumin as calibration standard. 10 μg of proteins for each sample were run on a sodium dodecyl sulfate-10% polyacrylamide gel under reducing conditions and then electrophoretically transferred onto nitrocellulose membranes (GE Healthcare, Milan, Italy). Blots were blocked 1h at room temperature with I-Block solution (Life Technologies Italia, Italy) in TBS + 0.1% Tween-20 buffer and then incubated with antibodies against the total proteins of interest. The conditions of the primary antibodies were the following: anti-RAB5 (1:2000, Cell Signaling Technology Inc., RRID: AB_823625), anti-RAB9 (1:2000, AbCam, RRID: AB_303323), anti-GALT (1:1000, AbCam, Cat# ab178406), anti-GM130 (1:1000, Sigma-Aldrich, RRID: AB_532244), and anti-β-Actin (1:10000, Sigma-Aldrich, RRID: AB_476697). Expression levels of every single protein were normalized using its own β-Actin loading control, which was detected by evaluating the band density at 43kDa. Optic density (OD) of immunocomplexes was visualized by chemiluminescence using the Chemidoc MP Imaging System (Bio-Rad Laboratories, RRID: SCR_008426). Gels were run two times each and the results represent the average from two different runs. We used a correction factor to average the different gels: correction factor gel 2 = average of (OD protein of interest/OD β-actin for each sample loaded in gel 1)/(OD protein of interest/OD β-actin for the same sample loaded in gel 2)(32).

Slice surface biotinylation

These experiments were performed as previously described (1, 3). Mice were anesthetized with isoflurane and decapitated. The brain was sectioned in cold carboxygenated HBSS enriched with 4mM MgCl, 0,7 mM $CaCl_2$ and 10 mM D-glucose, and equilibrated with 95% O2 and 5% CO2 to yield pH 7.4, on a vibrating microtome at a thickness of 300 μm. Dorsal striatum (STR) and prefrontal cortex (PFC) were dissected from coronal slices. Before starting the surface biotinylation reaction, and to ensure a gradual cooling of the cells, the tissues were washed twice for 5 minutes in ice-cold

HBSS buffer. The filters holding the tissues were transferred to a well containing an excess of biotinylation reagent solution of 100 µM NHS-LC-biotin (Pierce, Appleton, WI, USA) in HBSS. After 45 min of incubation, the tissues were transferred to another well and washed twice with HBSS buffer containing 200 mM Lysine (Sigma-Aldrich) to block all reactive NHS-LC-biotin in excess. The tissues were washed twice with ice-cold HBSS and immediately placed on ice to mechanically disrupt the tissue in 120 µl of lysis buffer (1% TX-100, PBS1X and a cocktail of protease inhibitors (Sigma-Aldrich). To discard extra debris, homogenates were centrifuged for 5 min at 4°C at 13.000 rpm and supernatants were collected. To precipitate the biotinylated proteins from the homogenates 50 µl of immobilized Streptavidin beads (Pierce) were added to the samples and the mixture was rotated for three hours at 4°C. The precipitates were collected by brief centrifugation, mixed with 50 µl of SDS-PAGE loading buffer, boiled for 5 minutes and stored at -80°C until use. Protein extracts were separated on precast 10% SDS/PAGE (Biorad, Milan, Italy) and transferred to nitrocellulose membranes. Blots were incubated with primary antibodies overnight at 4°C. Antibodies used were dopamine D2 receptor (sc-5303, Santa Cruz Biotechnology, Dallas, TX, USA, and AB5084P, Millipore), Synaptophysin (sc-365488, Santa Cruz Biotechnology) and Transferrin Receptor (sc-21011, Santa Cruz Biotechnology). Immune complexes were detected using appropriate peroxidase-conjugated secondary antibodies (Thermo Fisher Scientific) and a chemiluminescent reagent (ECL prime; GE Healthcare Europe GmbH, Milan, Italy). Densitometric analysis was performed by ImageQuantTL software (GE Healthcare Europe GmbH). Results were normalized to respective control conditions.

Stereotaxic injections

All surgeries were performed under aseptic conditions. Mice were deeply anesthetized by inhalation of a mixture of isoflurane/oxygen (2%/1%) and mounted into a stereotaxic frame (David Kopf Instruments, Tujunga, CA, USA). Following shaving and preparation of the skin, a cranial hole was made above the targeted area. All measurements were made relative to bregma, in accordance with the mouse brain atlas (33). The viral injection (60% AAV5.GfaABC1DcytoGCaMP6f.SV40, 40%

GfaABC1D.cyto-tdTomato.SV40, Addgene, Watertown, MA, USA) was performed using a borosilicate pipette at a rate of 50nl/min using a 10-µL Hamilton syringe. After each injection, 10-15 minutes were allowed before slowly withdrawing the micropipette.

Ex vivo calcium signaling in astrocytes

Coronal slices of 300 µm were obtained from mice at postnatal days 90-120 three weeks after AAV injections. Animals were anaesthetized with isoflurane and the brain was removed and transferred into an ice-cold artificial cerebrospinal fluid (ACSF, in mM: 125 NaCl, 2.5 KCl, 2 CaCl2, 1 MgCl2, 25 glucose, pH 7.4 with 95% O2 and 5% CO2). Coronal slices were cut with a vibratome (VT1000S, Leica Camera AG) in the solution described in (34). Then, slices were transferred for 1 minute in a solution at room temperature (RT, in mM: 225 D-mannitol, 2.5 KCl, 1.25 NaH2PO4, 26 NaHCO3, 25 glucose, 0.8 CaCl2, 8 MgCl2, 2 kynurenic acid with 95% O2 and 5% CO2). Finally, slices were transferred in sACSF at 32°C for 20 min and then maintained at RT for the entire experiment. To image Ca^{2+} dynamics in GCaMP6f-astrocytes, we used a two-photon (2P) laser scanning microscope (Multiphoton Imaging System, Scientifica Ltd., Uckfield, UK) equipped with a pulsed IR laser (Chameleon Ultra 2, Coherent, USA) tuned at 920 nm. Laser power at the sample was kept in the range 5–10 mW to avoid photostimulation and photobleaching. The excitation wavelength used was 920 nm for both GCaMP6f and tdTomato. Images were acquired at 1.53Hz acquisition frame rate, for 2 minutes, through a water-immersion objective (Olympus, LUMPlan FI/IR 20×, 1.05 NA). The field of view ranged between 700×700 µm and 120×120 µm depending on the zoom factor. Ca^{2+} signal recordings were performed in cortical layers II/III in PFC brain slices. Brain slices were continuously perfused in a submerged chamber at a continuous rate of 3 ml/min with the following (in mM): 120 NaCl, 2.5 KCl, 1 NaH_2PO_4, 26 $NaHCO_3$, 1 $MgCl_2$, 2 $CaCl_2$, 10 glucose, pH 7.4 (with 5% CO_2/95% O_2) at room temperature. Tetrodotoxin (1µM; Hellobio, Bristol, UK) was also added to the perfusion solution to block neuronal activity in all recordings. Detection of astrocyte region of interests (ROIs)

displaying Ca^{2+} elevations was performed with ImageJ in a semi-automated manner using the GECI-quant plugin (35). The software was used to identify ROIs corresponding first to the soma (>30 μm^2; confirmed by visual inspection), then to the proximal processes (>20 μm^2 and not corresponding to the soma) and finally to the microdomains (between 2 and 20 μm^2 corresponding to neither the soma nor the proximal processes). All pixels within each ROI were averaged to give a single time course of fluorescence values, F(t). Analysis of Ca^{2+} signals was performed with ImageJ (NIH) and a custom software developed in MATLAB 7.6.0 R2008 A (Mathworks, Natick, MA, USA)(36). To compare relative changes in fluorescence between different cells, we expressed the Ca^{2+} signal for each ROI as $\Delta F/F0=(F(t) - F0)/(F0)$. F0 was defined as the 15th percentile of the whole fluorescent trace for each ROI and considered as a global baseline. For each ROI we then defined as baseline trace the points of the $\Delta F/F0$ trace with absolute values smaller than twice the standard deviation of the overall signal. Significant Ca^{2+} events were then selected with a supervised algorithm as follows. Firstly, a new standard deviation was calculated on the baseline trace, and all local maxima with absolute values exceeding twice this new standard deviation were identified. Secondly, among these events, we considered significant only those associated with local Ca^{2+} dynamics with amplitude larger than fourfold the new standard deviation. The amplitude of each Ca^{2+} event was measured from the 20th percentile of the fluorescent trace interposed between its maximum and the previous significant one. Essentially, this procedure combines a threshold measured from the global baseline with a stricter threshold computed from a local baseline. We adopted this method to reduce artifacts from the recording noise superimposed on the slow astrocytic dynamics. All Ca^{2+} traces were visually inspected to exclude the ROIs dominated by noise. For each astrocyte we calculated the number of active ROIs, defined as the ROIs displaying at least one significant Ca^{2+} event, the frequency, i.e. the total number of Ca^{2+} events per minute and the mean amplitude of the Ca^{2+} events. For each parameter, we then calculated the mean value among all analyzed astrocytes.

Chromatographic analyses of dopamine, DOPAC, HVA, NA, 5HT, and 5HIAA

368 *Ex vivo tissue collection.* Brains were harvested following rapid decapitation and sliced in 1 mm
369 sections in a chilled stainless-steel mouse brain matrix. Slices were frozen on glass slides mounted
370 on dry ice. Using a 2 mm biopsy punch, bilateral PFC, STR and globus pallidus externus (GPe) tissues
371 were collected accordingly to the mouse brain atlas (33), and stored at -80°C until neurochemical
372 analyses.
373 *In vivo microdialysis.* Microdialysis procedure was performed as previously described (1, 3). A con-
374 centric dialysis probe with a dialyzing portion of 1 mm was prepared and stereotaxically implanted
375 in the right GPe (coordinates of the dialyzing portion tip, in mm, relative to bregma, according to the
376 atlas (33): anteroposterior (AP)=-0.4, lateral (L)=+1.9, ventral (V)=-4.5) under isoflurane anesthesia.
377 After surgery, mice were housed individually to recover for 24 hours. On the day of microdialysis,
378 probes were perfused at a constant flow rate (1 µl/min), with artificial cerebrospinal Fluid (aCSF, in
379 mM: 147 NaCl, 4 KCl, 2.2 $CaCl_2$) by means of a microperfusion pump. After 30 min stabilization,
380 samples were collected every 20 min and stored in dry ice until the end of the experiment. Three
381 groups of three dialysates (one hour per group) were consecutively collected: “baseline” (aCSF per-
382 fusion), “quinpirole” (perfusion of 25 nM quinpirole), and “wash-out” (aCSF perfusion). At the end
383 of the microdialysis experiment, brains were collected and sliced to check probe implantation; only
384 data obtained from mice with probes correctly implanted in GPe were included in the results.
385 *Quantification of monoamines and metabolites by HPLC.* PFC, STR, and GPe tissue samples were
386 lysed by sonication in 0.1 M perchloric acid, and centrifuged (15,000 x g, 10 minutes, 4°C). The
387 supernatant was filtered by centrifugation (20,000 x g, 5 min, 4°C) in ultra-free microcentrifuge tubes
388 (Millipore, Burlington, Massachusetts, USA). Supernatants obtained from PFC, STR or GPe samples,
389 and from dialysates obtained from GPe *in vivo* microdialysis were injected (11 µl) into a high-perfor-
390 mance liquid chromatography apparatus (Alexys UHPLC/ECD Neurotransmitter Analyzer, Antec
391 Scientific, Zoeterwoude, The Netherlands), equipped with an autosampler (AS 100 UHPLC, micro,
392 6-PV, Antec Scientific). The mobile phase [containing (in mM) 100 phosphoric acid, 100 citric acid,
393 0.1 EDTA.2H $2H_2O$, 3 octanesulfonic acid. NaCl plus 8% acetonitrile, adjusted to pH 3.0 with NaOH

394 solution (50%)] was delivered at 0.050 ml/min flow rate with a LC 110S pump (Antec Scientific)
395 through an Acquity UPLC HSS T3 column (1 x 100 mm, particle size 1.8 µm; Waters, Milford,
396 Massachusetts, USA). Detection of dopamine, DOPAC and HVA was confirmed and carried out with
397 two system. An electrochemical detector (DECADE II, Antec Scientific) equipped with a SenCell 2
398 mm glassy carbon working electrode (Antec Scientific) set at +600 mV versus Ag/AgCl. Output sig-
399 nals were recorded with Clarity (Antec Scientific). The second HPLC was equipped with a reversed-
400 phase column (C8 3.5 um, Waters, USA) and a coulometric detector (ESA Coulochem III; Agilent
401 Software). The electrodes of the analytical cell were set at +350 mV (oxidation) and −200 mV (re-
402 duction). The mobile phase contained 50 mM CH_3COONa, 0.07 mM Na_2EDTA, 0.5 mM n-octyl
403 sulfate, and 12% (v/v) methanol, the pH of mobile phase was adjusted with CH_3COOH to 4.21. The
404 sensitivity of the assay for DA/DOPAC/HVA was 5 fmol/sample. For tissue sample analysis, data
405 were normalized by tissue weight. Dialysate contents were converted into percentages of the average
406 baseline level calculated from the three fractions of the first hour of collection ("baseline" period),
407 and are expressed as averaged percentages of "baseline", "quinpirole" and "wash-out" periods, ob-
408 tained in each experimental group.
409
410 **Drosophila**
411 ***Stocks and crosses.*** The UAS-Ddysb-RNAi *Drosophila* line (v34355) used in this study was obtained
412 from VDRC (Vienna Drosophila Stock Center). The Gal4 activator lines tubulin-Gal4 (5138), repo-
413 Gal4 (7415), and elav-Gal4 (458), and the transgenic lines UAS-GalT-GFP (30902), were obtained
414 from the Bloomington Stock Center, Indiana University. Experimental crosses were performed at
415 28°C.
416 ***Immunochemistry***. *Drosophila* immunostaining was performed on wandering third instar larvae
417 reared at 28°C. Third-instar larvae were dissected in PBS and fixed in 4% paraformaldehyde (PFA)
418 in PBS for 15 minutes, washed in PBS 0,1% Triton X-100 (PBTX), and incubated with primary an-
419 tibody overnight, and secondary antibody for 1 hour. The primary antibody anti-Repo-8D12 (1:200,

DSHB) and anti-ELAV (1:200, DSHB) were used. Secondary antibody Cy5coniugated Goat anti-Mouse IgG (115-175-003) was from Jackson Immuno Research, and was used at 1:500. Third instar larvae were then mounted with Mowiol 488 and imaged using a Nikon EZ-C1 confocal microscope equipped with a Nikon Plan APO 60.0×/1.40 oil immersion objective. Z-stacks with a step size of 1 µm were taken using identical settings. Each stack consisted of 15 to 20 plane images of 10 animals per genotype. The images obtained were processed and analyzed using *ImageJ*.

qRT-PCR. *Drosophila* samples (8 mg each) were homogenized and total RNA was subsequently isolated as in (37). Quantification of D2R gene expression was performed on Eco Real-Time PCR (Illumina, San Diego, CA, USA) using One Step SYBR PrimeScript RT-PCR II kit (Takara Bio, Shiga, Japan). The expression level of RP49 was used as a housekeeping (normalizing) gene. Relative gene expression was quantified with the ΔΔCt Comparative method. The primers used for expression of D2R gene were: forward primer, 5'-CCTTCTACAACGCCGACTTTA-3', reverse primer 5'-ACTCCTCAGCGCCTTGAA-3'. To avoid eventual contamination by genomic DNA primers were designed to span an intron–exon boundary and RNA samples were treated with DNase.

Electron microscopy. The TEM projections images of Drosophila brains were acquired from ultra-thin sections under a FEI Tecnai-12 transmission electron microscope (FEI Netherlands) as in (38).

Human samples

The mRNA expression values are referred to DTNBP1 NM_183040 gene expression in the human postmortem dorsolateral prefrontal cortex (DLPFC) of normal subjects across lifespan. The data are available in the open access on-line application "The Brain Cloud", which allows the query of genome-wide gene expression data and their genetic control, http://www.libd.org/braincloud. We selected the single isoform values on the base of Illumina probes used for the quantification. The Illumina probes used to identify the human dysbindin-1 isoforms were, for Dysbindin-1A hHA -

chr6:15632467-15632536, and for Dysbibdin-1C the hHC -chr6:15735609-15735678, both referred to Human Assembly March 2006 (NCBI 36/hg18).

Caudate samples from 18 healthy control samples and 22 schizophrenia cases were obtained from the NSW Tissue Resource Center. The tissue was processed at Neuroscience Research Australia as approved by the University of New South Wales Human Research Ethics Committee (HREC 12435; Sydney, Australia). No significant differences were found in the demographic variables of age, sex, pH, or PMI between the diagnostic groups (Supplementary Fig. S6). The rostral caudate was dissected from anatomically matched fresh frozen coronal sections cut at 60 μm through the head of the caudate. Caudate extracted samples (run in duplicates) were denatured in loading buffer 2X, and boiled for 5 min at 95°C, then the denatured samples were centrifuged at 10,000 g for 5 min. Each lane was loaded with 20 mg of total protein, as in previous studies (Talbot et al. 2011; Tang et al. 2009).

Statistics

For animal experiments, no statistical methods were used to predetermine sample sizes, although sample sizes were consistent with those from previous studies (1, 3, 29, 39). No explicit randomization method was used to allocate animals to experimental groups and mice were tested and data processed by investigators blind to animal identity. Statistical analyses were performed using commercial software (STATISTICA- 13.5, StaSoft, Tulsa, OK, USA, and Prism 7, GraphPad, San Diego, CA, USA). Results are expressed as mean ± standard error of the mean (SEM) throughout. Multiple Student's *t*-tests, one-way and two-way ANOVAs were used, as appropriate. The accepted value for significance was $P<0.05$. Newman-Keul's test for post hoc analysis was performed once ANOVA highlighted a statistical significance for main effects. Data distribution was tested using the D'Agostino and Pearson normality test. The experiments reported in this work were repeated independently two to four times, using mice from at least four different generations. Numbers of mice are reported in the figure legends.

Results

Dys1 hypofunction alters astrocytic reactivity

Unbiased microarray analysis showed increased expression of reactive astrogliosis-related genes in Dys1 knockout mice compared to wild-type Dys1+/+ (Fig. 1a and Supplementary Fig. S1). Thus, to better investigate if Dys1 regulates astrocytic activity in mammals, we used Dys1 heterozygous mice (Dys1+/-), a model with direct translational validity for both healthy human subjects and patients with schizophrenia (1, 3).

Microarray indication was confirmed by higher immunoreactivity of the astroglial marker glial fibrillary acid protein (GFAP) in Dys1+/- compared to Dys1+/+ littermates (Fig. 1b), which was similarly evident in prefrontal cortex (PFC), and basal ganglia (NAcc, dorsal striatum: STR, GPe) regions (Fig. 1c).

By two-photon laser scanning microscope experiments in slice preparations from Dys1+/+ and Dys1+/- mice we next evaluated Ca^{2+} signal dynamics in GCaMP6f-expressing astrocytes (Fig. 1d). We found that the number of spontaneous Ca^{2+} events occurring in astrocyte fine distal processes (i.e. microdomains) was markedly increased in Dys1+/- mice compared to Dys1+/+ mice, while the mean Ca^{2+} peak amplitudes was unchanged (Fig. 1e, f, g). Ca^{2+} activity at soma and proximal processes showed no significant differences (Fig. 1e, f, g). These results confirm a hyperactivity of astrocytes in Dys1 hypofunctioning mice.

Overall, these data provide initial evidence that reduced levels of Dys1 alter astrocyte microdomain signals.

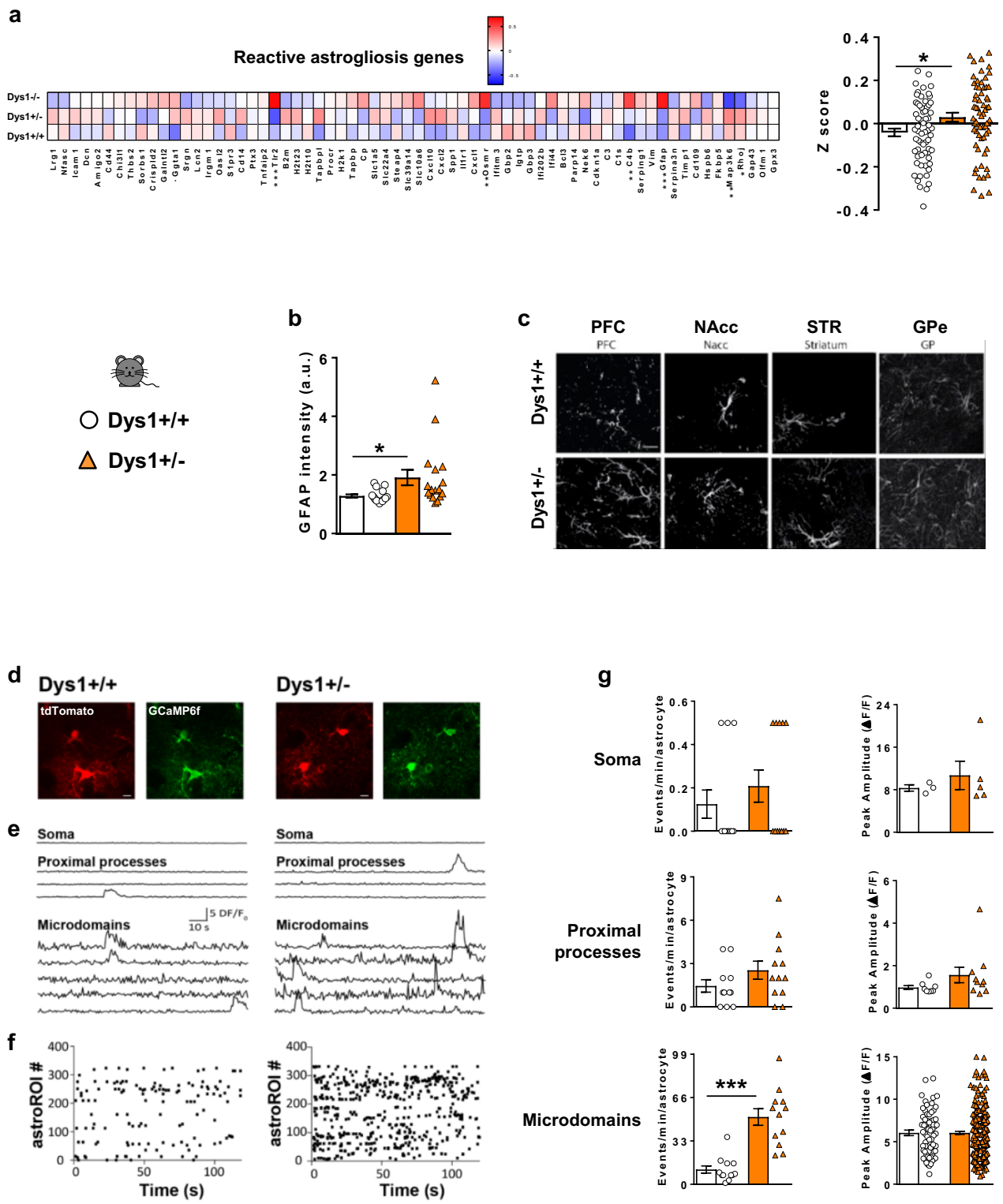

Figure 1. Dys1 modulates astrocytic reactivity. a. Heat map of 65 inflammatory markers selected by a microarray screening from Dys1+/+ (n24), and Dys1+/- (n25) littermates. The heat map is based on hierarchical clustering of genes involved in inflammation states. All gene expression levels were transformed to scores ranging from −0.5 to 0.5 and were colored blue, white, or red to represent low, moderate, or high expression levels, respectively. The relative expression levels were scaled based on their mean and do not represent expression levels in comparison with controls. Dys1+/- mice show higher expression for these genes compared to Dys1+/+ littermates (t-test: t_{128}=-2.23, p=0.028). *p<0.05 vs Dys1+/+. **b.** Quantification of cumulative GFAP intensity from confocal images from

PFC, NAcc, STR and GPe displayed by Dys1+/+ and Dys1+/- littermates (n4/genotype, 1/brain region averaged from 9 samples each). Scale bars, 20μm (t-test: t_{31}=-2.32, p=0.027) *p<0.05 vs Dys1+/+. **c.** Representative confocal images of GFAP positive astrocytes in the analyzed brain regions. **d.** Two-photon images (average fluorescence of 2min acquisition) of tdTomato (red) and GCaMP6f (green) expressing astrocytes in cortical slices from Dys1+/+ and Dys1+/- mice. Scale bars, 10 μm. **e.** Representative Ca^{2+} signal traces from the main astrocytic compartments. **f.** Raster plots of Ca^{2+} transients from all GCaMP6 astrocyte microdomains in Dys1+/+ and Dys1+/- mice. **g.** Mean number of events per minute per astrocyte and mean peak amplitudes of Ca^{2+} transients per active ROI in Dys1+/+ and Dys1+/- astrocytes (11 for Dys1+/+ and 12 for Dys1+/- mice, 4 animals each; microdomain events: t-test: t_{22}=-5.83, p<0.0001). ***p<0.0001 vs Dys1+/+. Bar graphs show mean±s.e.m.

Distinct neuronal/astrocytic expression and developmental patterns of Dys1 isoforms

We then asked whether Dys1 isoforms might be differentially expressed in neurons and astrocytes.

Dys1A was expressed in adult mouse brain, in cultured astrocytes cells, and in cultured neuronal cells (Fig. 2a). In contrast, Dys1C was missing in astrocytes cells, while its expression was higher than Dys1A in the brain as well as in cultured neuronal cells (Fig. 2a). Dys1A showed a stable expression over time in glial and neuronal cultures, while Dys1C was always absent in astrocytes cultures and increased its expression over time in neuronal cells (Fig. 2b,c). We confirmed divergent developmental patterns of expression of these two Dys1 isoforms, with similar findings in human and mouse brains. Specifically, samples of human dorsolateral PFC revealed higher Dys1A expression in the embryonic phase, which gradually decreased across development (Fig. 2d). Conversely, Dys1C expression was lower in embryonic and childhood stages and then increased from adolescence (Fig. 2d). Similarly, in mouse PFC the expression of Dys1A protein decreased from the embryonic phase, while Dys1C increased its expression in adolescence (Fig. 2e).

Overall, these data show a similar developmental pattern of Dys1 isoforms expression between mice and humans, and define a previously unexpected constraint of Dys1A expression in astrocytes.

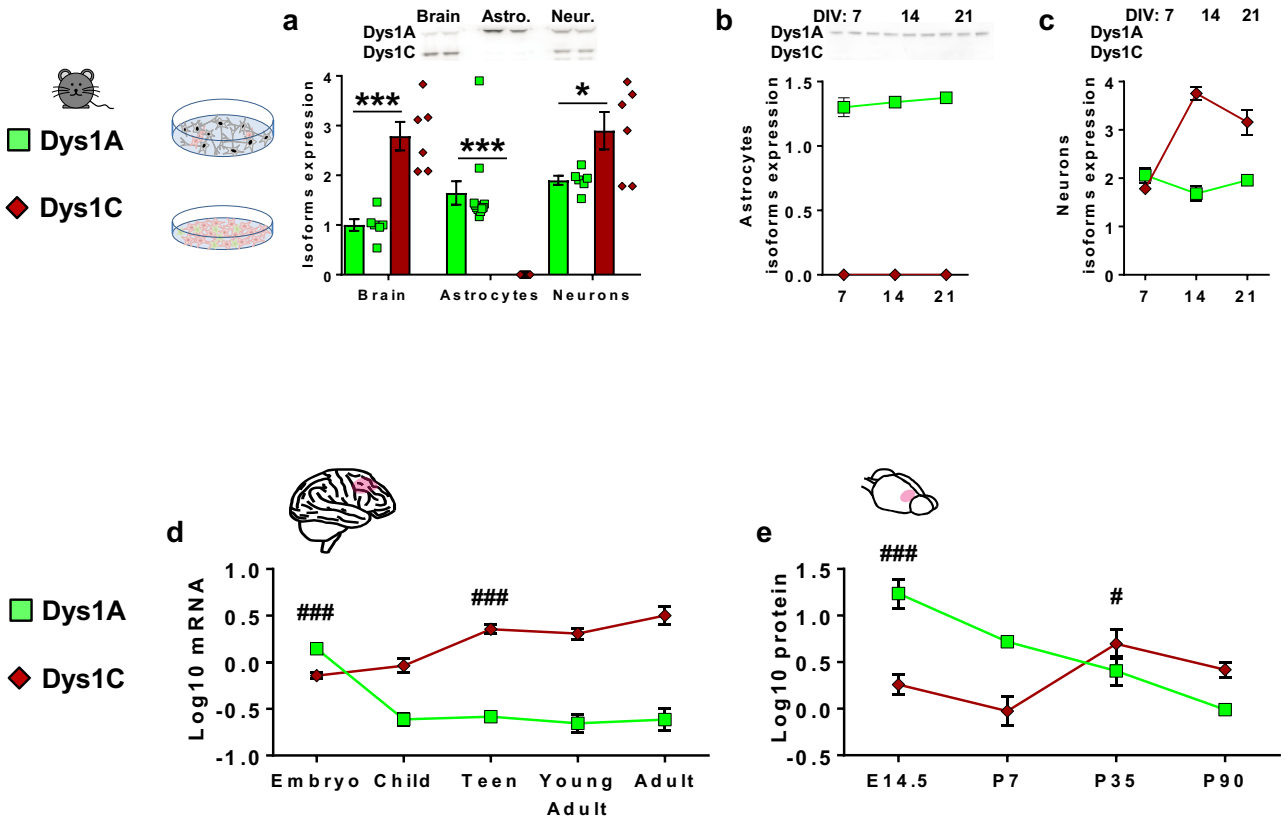

Figure 2. **Neuronal and astrocytic expression and developmental patterns of Dys1 isoforms. a.** Representative western blots and densitometric analysis of Dys1A (50 kDa) and Dys1C (38 kDa) isoforms. β-actin used as loading control. In brain lysate of adult PND90 mice both isoforms were revealed, with higher expression for Dys1C compared to Dys1A (t-test: t_{10}=-5.77, p=0.0002). Dys1A was the only isoform expressed in glial cells (t-test: t_{20}=-6.32, p<0.0001). Similar to brain lysate, neuronal cultures show the expression of both isoforms with relative higher levels of Dys1C (t-test: t_{10}=-2.57, p=0.02). **b.** Astrocytes cultures at different developmental time points (day 7=DIV7; day 14= DIV14; day 21= DIV21) confirming no expression of Dys1C in astrocytes. **c.** Neuronal cultures at different developmental time points (DIV7, 14 and 21) showing relative higher expression of Dys1C compared to Dys1A. **d.** mRNA expression of Dys1A and Dys1C isoforms from the human dorsolateral PFC by the open-access Brain Cloud databank at different developmental ages. Ns: Embryos=38; Child=32; Teen=50; Young adult=25; Adult=122. Dys1A expression was highest at the embryonic stage and then decreased, while Dys1C expression increased from adolescence (two-way ANOVA, isoforms*age interaction: $F_{5,250}$=68.84; p<0.0001). $^{###}$p<0.0001 vs consecutive ages for Dys1A, and vs preceding ages for Dys1C. **e.** Protein expression of Dys1A and Dys1C isoforms from the mouse prefrontal cortex at different developmental ages. n6 mice/time point. Dys1A expression was highest at the embryonic stage and then decreased, while Dys1C expression increased from adolescence (two-way ANOVA, isoforms*age interaction: $F_{3,17}$=32.77; p<0.0001). $^{#}$p<0.01 and $^{###}$p<0.0001 vs consecutive ages for Dys1A, and vs preceding ages for Dys1C. Bar graphs show mean±s.e.m.

Dys1A disruption alters basal ganglia- but not cortical-dependent behaviors

The observation that only the Dys1A isoform is expressed in astrocytes prompted us to explore the effects of a selective Dys1A disruption using a mouse line with flanking LoxP sites targeted to the exon 5 of Dtnbp1 on chromosome 13a ($Dys1A^{flox/flox}$), backcrossed with a germline Cre deleter mouse line (26).

Dys1A+/- and Dys1A-/- mice have a gene dosage-dependent reduction and lack of Dys1A isoform, respectively, and unaltered Dys1C expression (Fig. 3a and Supplementary Fig. S2). We then performed in Dys1A knockout mice a comprehensive battery of behavioral tests that were previously applied to mice with disruption of both Dys1 isoforms (1, 3, 40, 41).

In agreement with an initial characterization (26), Dys1A+/- and -/- mice were viable with no evident alterations in general health and sensory functions. Similar to this previous study, Dys1A-/- mice presented a hyperactive phenotype compared with Dys1A+/+ littermates (Fig. 3b), as in Dys1 knockout mice (1, 41). Moreover, as in Dys1 knockout mice (41), locomotor responses to both acute and sub-chronic amphetamine were not affected by deletion of Dys1A (Supplementary Fig. S2). I these mice, in contrast to Dys1 knockout mice (40, 42, 43), no Dys1A-dependent alterations were evident in sociability and social memory (Fig. 3c,d). These results indicate that Dys1A is involved in locomotor activity, but not in social interactions.

Dys1 hypofunction is associated with PFC-dependent executive functions deficits in mice, healthy humans, and patients with schizophrenia (1, 3). Thus, we tested Dys1A mice in the attentional set-shifting task (ASST), which allows assessment of discrete cognitive executive functions with translational validity to humans (3, 28). In contrast to Dys1 knockout mice (1, 3), Dys1A+/- and -/- mice show no deficits in extradimensional set-shifting (EDS) but serial reversal learning was altered (Fig. 3e,f). EDS alterations imply dopaminergic dysfunction in PFC (28, 44), while serial reversal learning is linked to dopaminergic tone in striatal regions (28, 45). This prompted us to assess behaviors more related to basal ganglia dopamine-related functioning.

Prepulse inhibition (PPI) deficits are consistently linked to overactive dopamine/D2 signaling in basal ganglia (46-48). We found a gene-dosage effect for reduced PPI in Dys1A+/- and -/- compared with Dys1A+/+ littermates (Fig. 3g). No Dys1A-dependent effects were evident for acoustic startle responses or body weight (Supplementary Fig. S2), excluding potential confounding factors.

Motivation to receive a reward is another behavioral trait strongly related to dopaminergic functioning within the basal ganglia (49-51). We found reduced reward-motivated behavior in Dys1A+/- and -/- compared with Dys1A+/+ littermates (Fig. 3h), when tested in a progressive ratio paradigm designed to assess motivational processes (30). No Dys1A-dependent differences were present during acquisition phases (Supplementary Fig. S2), excluding deficits in motor coordination, learning and memory.

Overall, these findings point to a prominent involvement of Dys1A in behavioral phenotypes mediated by dopaminergic signaling in the basal ganglia (Fig. 3i).

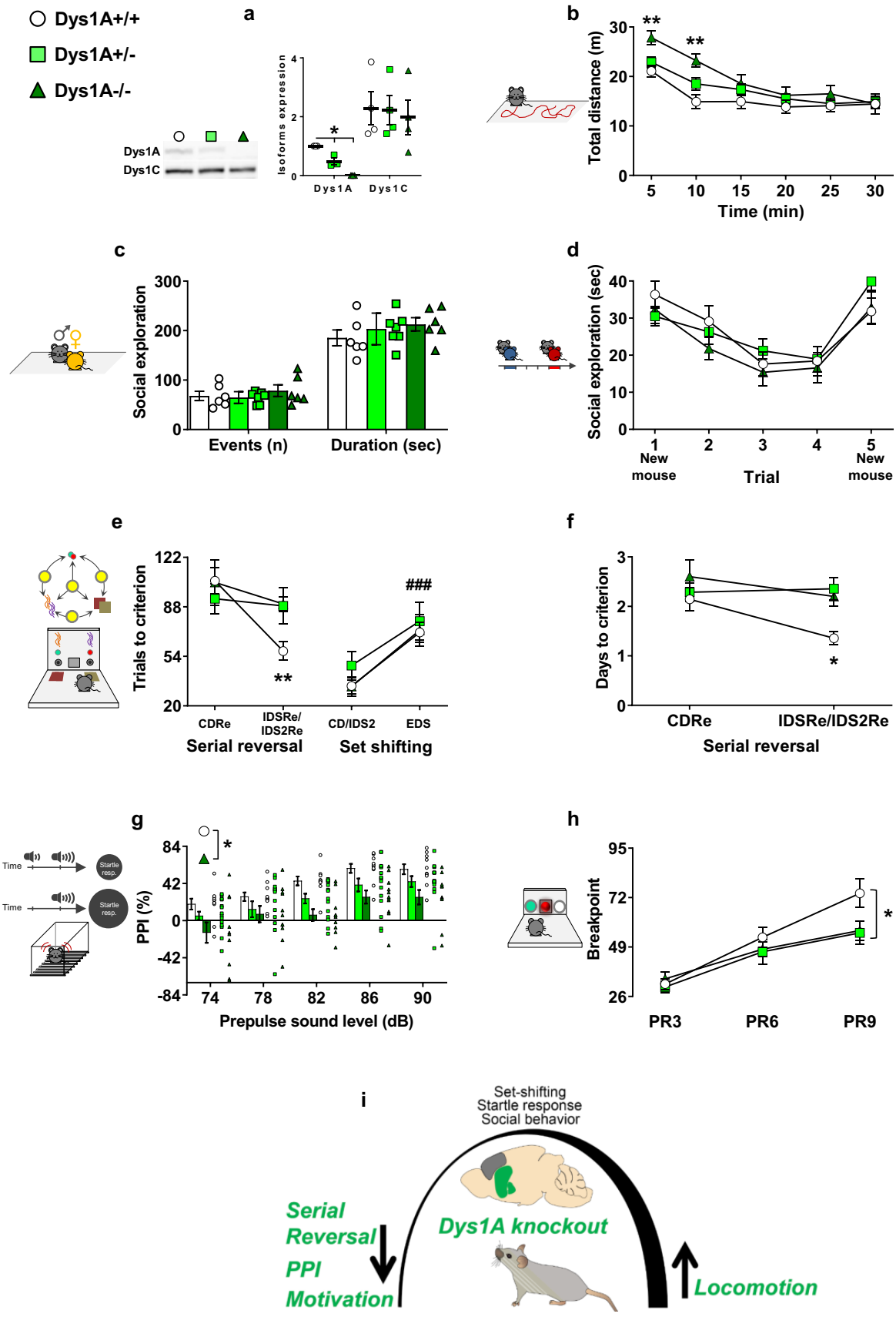

588

589 **Figure 3. Dys1A disruption impairs basal ganglia- but not PFC-dependent behaviors. a.** Selec-
590 tive reduction of Dys1A does not affect Dys1C expression. Western blots and densitometric analysis
591 in Dys1A+/+, +/- and -/- littermates. Expression of Dys1A (50 kDa), Dys1C (38 kDa). β-actin used

as loading control. Expression of Dys1A is reduced in Dys1A+/- and absent in Dys1A-/- in PFC (one-way ANOVA, $F_{2,6}$=60.48; p<0.0005). *p<0.01 vs Dys1A+/+ littermates. Expression of Dys1C was intact across all genotypes (one-way ANOVA, $F_{2,9}$=0.09; p=0.92). n4 mice/group. **b.** Spontaneous distance traveled by Dys1A+/+ (n17), Dys1A+/- (n22) and Dys1A-/- (n10) during 30-min exposure to an open field arena. Dys1A-/- show increased locomotion during the first 10 min in the open field (Two-way repeated measure ANOVA, time*genotype interaction: $F_{10,215}$=3.04; p=0.001). **p<0.005 vs Dys1A+/+ at the same time point. **c.** Male-female social interaction, displayed by Dys1A+/+ (n6), Dys1A+/- (n7) and Dys1A-/- (n6) littermates. No genotype-dependent difference was evident in the number of events or exploration time (two-way ANOVA; events: $F_{2,15}$=0.52; p=0.60; duration: $F_{2,15}$=0.75; p=0.49). **d.** Social habituation-dishabituation, displayed by Dys1A+/+ (n14), Dys1A+/- (n16) and Dys1A-/- (n10) littermates. No genotype-dependent difference was evident (two-way repeated measure ANOVA genotype: $F_{2,37}$=0.37; p=0.69; genotype*time interaction: $F_{8,148}$=1.88; p=0.07). **e.** Attentional Set-Shifting Test (ASST), performed in Dys1A+/+ (n14), Dys1A+/- (n14) and Dys1A-/- (n10) littermates. In contrast to Dys1A+/+, both Dys1A+/- and Dys1A-/- mice did not show the expected reduced trials to criterion in serial reversal stages (two-way repeated measure ANOVA; reversal stage: $F_{1,35}$=11.46; p=0.002; genotype*reversal stage interaction: $F_{2,35}$=4.27; p=0.02). **p<0.005 vs Dys1A+/- and -/- at the same time point. All mice showed the expected increase in trials to criterion at EDS stage independent of genotype (two-way repeated measures ANOVA; shifting stage: $F_{1,35}$=17.45; p=0.0002; genotype*shifting stage interaction: $F_{2,35}$=0.09; p=0.92). ###p<0.0005 vs CD/IDS2 stages. **f.** Days needed to reach criterion in ASST stages shown by Dys1A+/+ (n14), Dys1A+/- (n14) and Dys1A-/- (n10) littermates. In contrast to Dys1A+/+ mice, both Dys1A+/- and Dys1A-/- mice did not show the expected reduced days to criterion in serial reversal stages (two-way repeated measure ANOVA; reversal stage: $F_{1,35}$=5.01; p=0.03; genotype*reversal stage interaction: $F_{2,35}$=2.60; p=0.05). **g.** Percent PPI of the 120dB acoustic startle response displayed by Dys1A+/+ (n10), Dys1A+/- (n15) and Dys1A-/- (n12) littermates. Dys1A-/- have lower PPI compared to Dys1A+/+ mice (two-way repeated measure ANOVA; genotype: $F_{2,34}$=4.44 p=0.019). *p<0.01 vs Dys1A+/+. **h.** Breakpoint during a food-driven operant behavior test with increasing progressive ratio (PR) displayed by Dys1A+/+ (n12), Dys1A+/- (n13) and Dys1A-/- (n10) littermates. Both Dys1A+/- and Dys1A-/- mice showed lower breakpoints than Dys1A+/+ mice (two-way repeated measures ANOVA; genotype: $F_{4,64}$=2.8; p=0.032). *p<0.05 vs Dys1A+/+. Bar and line graphs show mean ± s.e.m. **i.** Schematic drawing summarizing the behavioral data obtained in Dys1A knockout mice, pointing to a major alteration of basal ganglia-dependent, but not PFC-dependent, phenotypes.

Dys1A disruption alters dopamine/D2 homeostasis in basal ganglia but not in PFC

Dopaminergic signaling in basal ganglia is implicated in locomotion, motivation, serial reversal learning, and PPI (45, 46, 48), which are altered in Dys1A knockout mice. Thus, we assessed Dys1A modulation of dopaminergic system in basal ganglia and, as comparison, in PFC.

We first revealed a higher expression of Dys1A protein in GPe compared to PFC and STR (Fig. 4a). Notably, GPe is an astrocyte-enriched brain region (20). In contrast, Dys1C was equally expressed in all regions considered (Fig. 4b).

Dys1A disruption increased the expression of total D2 receptors in GPe, but not in PFC or STR (Fig. 4c). Moreover, Dys1A disruption increased cellular surface D2 receptors in STR and GPe, but not in PFC (Fig. 4d). Notably, disruption of both Dys1 isoforms resulted in comparable D2 alterations, but both in PFC and striatal regions (1, 3) Supplementary Fig. S3). Similarly, a Dys1A genotypic effect on dopamine content was present in STR and GPe, but not in PFC (Fig. 4e-g). In particular, Dys1A-/- mice had lower dopamine levels than Dys1A+/+ in both STR and GPe, and lower HVA levels in STR (Fig. 4f-g). DOPAC/dopamine and HVA/dopamine ratios were indistinguishable across genotypes in all regions, suggesting a normal rate of dopamine catabolism (Supplementary Fig. S3). No Dys1A genotype effects on levels of noradrenaline, serotonin, and 5HIAA were evident (Supplementary Fig. S3).

Consistent with our behavioral assessments, our data show that the selective disruption of the Dys1A isoform alters the dopaminergic system in basal ganglia, but not in PFC.

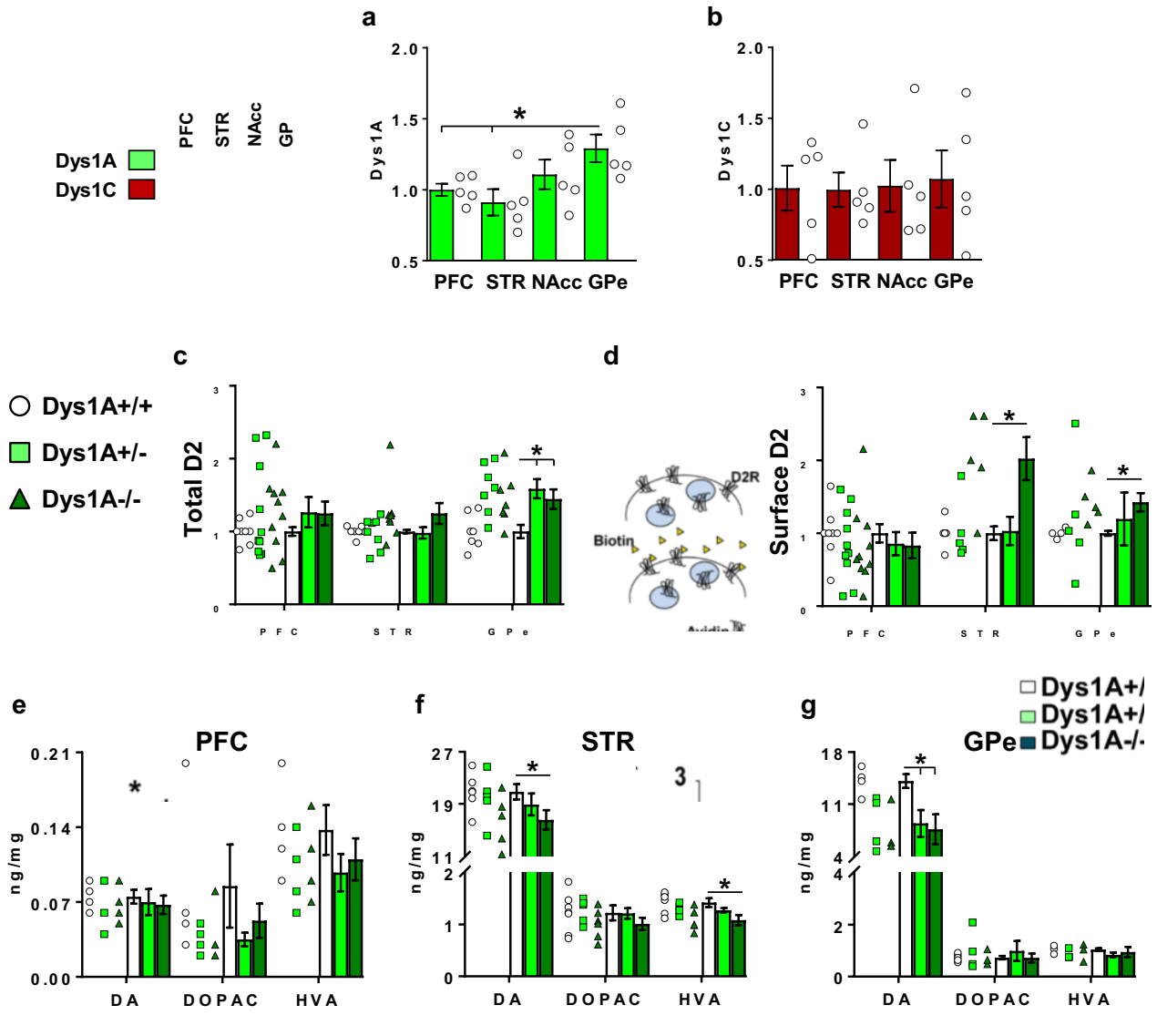

Figure 4. Dys1A alters the dopaminergic system within basal ganglia but not PFC. Protein expression displayed by C57BL6J adult mice of **a.** Dys1A and **b.** Dys1C isoforms in the PFC, STR, NAcc, and GPe relative to PFC and normalized to their own β-actin. Dys1A expression is higher in GPe compared to PFC and STR (one-way ANOVA: $F_{3,16}$=5.02; p=0.02). *p<0.05 vs PFC and STR. Dys1C expression is uniform across the selected brain areas (one-way ANOVA: $F_{3,16}$=0.045; p=0.98). **c-d.** D2 receptor expression in Dys1A+/+ (n9), Dys1A+/- (n10) and Dys1A-/- (n10). Synaptophysin was used as cytoplasmic control, and D2 expression normalized on transferrin as loading control. **c.** Dys1A+/- and Dys1A-/- mice show increased total D2 expression compared to Dys1A+/+ in GPe (one-way ANOVA: $F_{2,16}$=4.93; p=0.021), but not in PFC ($F_{2,25}$=0.724; p=0.49), and STR (one-way ANOVA: $F_{2,22}$=1.44; p=0.26). **d.** Biotinylation protocol for brain slices treated with biotin to label all surface proteins, precipitated by streptavidin. Dys1A-/- mice have increased expression of D2 receptors on cellular surface compared to Dys1A+/+ littermates in STR and GPe (one-way ANOVA: STR $F_{2,14}$=4.20; p=0.04; GPe $F_{1,6}$=6,18; p=0.04), but not in PFC (one-way ANOVA: $F_{2,24}$=0.44; p=0.64). *p<0.05 vs Dys1A+/+. **e-g.** Dopamine (DA), DOPAC, and HVA content by HPLC, expressed as ng/mg of tissue in **e.** PFC, **f.** STR, and **g.** GPe dissected from Dys1A+/+ (n4), Dys1A+/- (n4), and Dys1A-/- (n4) littermates. No Dys1A-dependent changes were observed in PFC (one-way ANOVA: $F_{2,5}$=0.23; p=0.80). Dys1A-/- show reduced DA and HVA levels relative to Dys1A+/+ in the STR (one-way ANOVA: $F_{1,10}$=5.17; p=0.05). Dys1A+/- and Dys1A-/- show reduced DA levels relative to Dys1A+/+ in GPe ($F_{1,10}$=10.44; p=0.02). *p<0.05 vs Dys1A+/+. Bar graphs show mean±s.e.m.

666

Dys1A hypofunction alters Golgi trafficking in astrocytes, but not in neurons

Dys1 influences the dopaminergic system by altering intracellular vesicular trafficking (16, 52, 53). Thus, we first checked different markers of vesicular trafficking in GPe of Dys1A knockout mice. Our focus on GPe was driven by Dys1A-dependent dopaminergic alterations prevalently in this region (Fig. 4), and because this is an astrocyte-enriches area (20).

Dys1A disruption decreased the expression of Rab5 (Fig. 5a, Supplementary Fig. S4), that regulates the internalization and trafficking of membrane receptors (vesicle fusion and receptor sorting in the early endosomes), and Rab9 (Fig. 5b, Supplementary Fig. S4), a protein that mediates endosome-to-trans-Golgi Network (TGN) transport (54, 55). Similarly, the trans-Golgi marker Galt (56) as well as the cis-Golgi marker GM130 (57) were both reduced in Dys1A knockout mice (Fig. 5c,d, Supplementary Fig. S4). These data indicate that disruption of the single Dys1A isoform is sufficient to generate alterations in vesicular trafficking within the basal ganglia.

Using electron microscopy analyses, we then investigated if there could be any visible Dys1A-dependent morphological alteration in intracellular vesicles that differ between neuronal and astrocytic cells. Compared to Dys1A+/+, we found in Dys1A-/- mice more irregularly shaped and swollen cisternae of the Golgi complex with enlarged vesicle-like structures in astrocytic, but not neuronal cells (Fig. 5e and Supplementary Video V1). In contrast, deletion of all Dys1 isoforms disrupted Golgi complex morphology in an equivalent way, but in both neuronal and astrocytic cells (Fig. 5f). Equivalent results in altered Golgi complex morphology were obtained by knocking down drosophila dDys either ubiquitously (Fig. 5g) or in glial cells and no obvious dysfunctions were observed in neuronal reduction (Supplementary Fig. S5). These findings further support a more prominent role for Dys1A in basal ganglia astrocytic functioning.

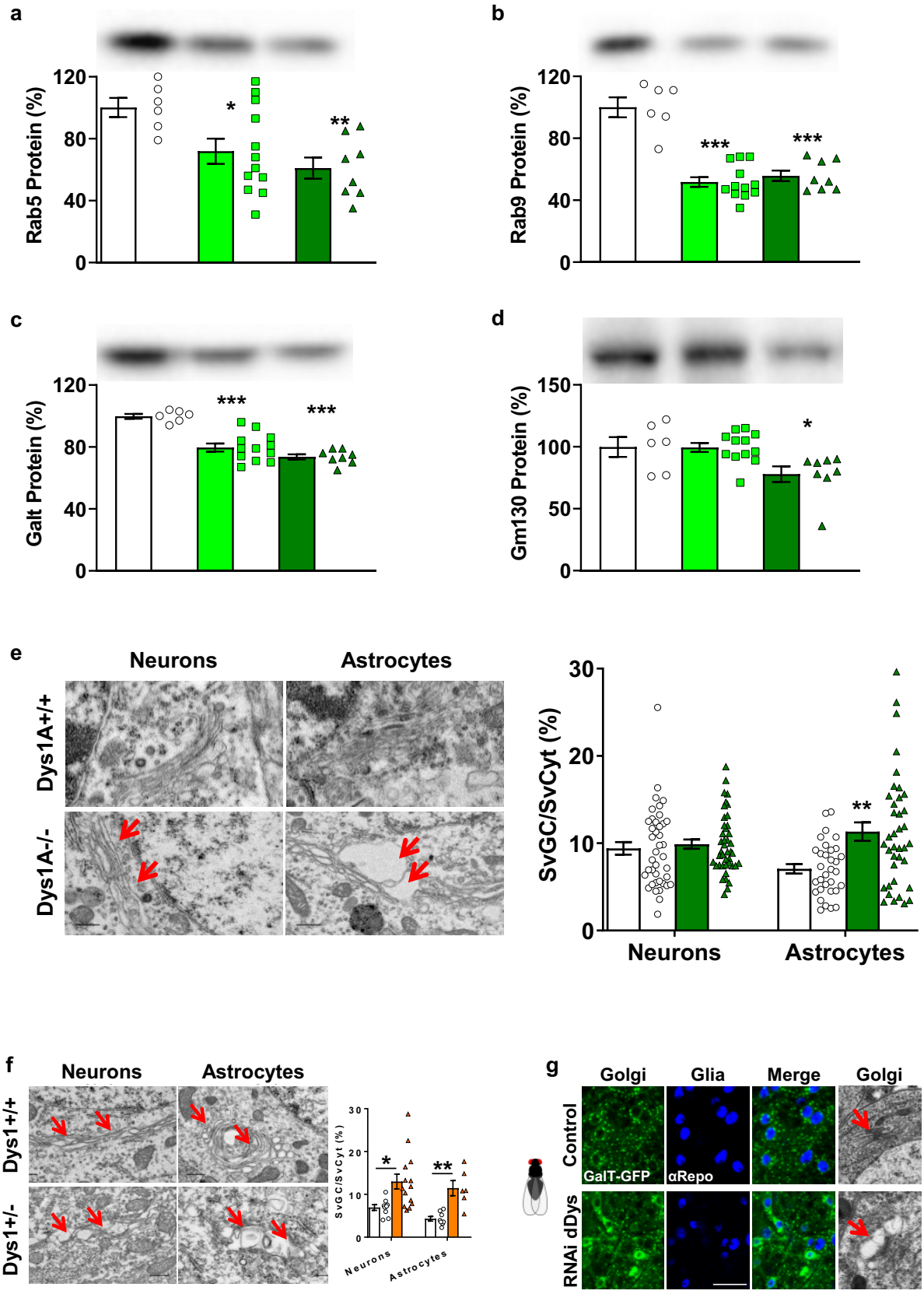

Figure 5. Dys1A disruption alters vesicular trafficking and Golgi complex morphology in basal ganglia astrocytes. a. Rab5, **b.** Rab9, **c.** GALT, and **d.** GM130 protein levels in the whole homogenate of GPe from Dys1A+/+ (n=6), Dys1A+/- (n=12) and Dys1A-/- (n=8) mice. Protein expression of Rab5, Rab9, GALT and GM130 are reduced in both Dys1A+/- and Dys1A-/- mice (One-way ANOVA: Rab5: $F_{2,23}$=5.01; p=0.016; Rab9: $F_{2,23}$=36.24; p<0.0001; GALT: $F_{2,23}$=27.34; p<0.0001;

GM130: $F_{2,23}$=5.21; p=0.014). Bar graphs show mean±s.e.m.and are expressed as percentages of Dys1A+/+ mice. Representative immunoblots are shown below each graph (complete immunoblots in Supplementary Fig. S4. *p<0.05, **p<0.01, ***p<0.001 vs Dys1A+/+ mice, ## p<0.01 vs Dys1A+/- mice. **e.** Representative transmission electron microscopy (TEM) images of the Golgi Complex (GC, red arrows) from Dys1A+/+ and Dys1A-/- littermates in neuronal and astrocytic cells. Surface density of GC (SvGC/SvCyt) in Dys1A-/- was not altered in neurons (t-test: t_{80}=-0.54, p=0.59), but increased compared with Dys1A+/+ control mice in astrocytic cells (t-test: t_{68}=-3.38, p<0.001). **p<0.001 vs Dys1A+/+ littermates. **f**. Transmission electron microscopy (TEM) images of the Golgi Complex (GC) in neurons and astrocytes in Dys1+/+ and Dys1+/- littermates. Surface density of GC (SvGC/SvCyt) in Dys1+/- mice was significantly higher than in Dys1+/+ littermates (neurons t_{21}=-2.70, p=0.013; astrocytes t_{12}=-4.40, p=0.0009). *p<0.05, **p<0.001 vs Dys1+/+. **g.** Maximum intensity projections of ventral ganglion cells, from Drosophila third instar larvae expressing UAS-GalT-GFP to visualize Golgi cisternae, for controls (tubulin-Gal4/+) and UAS-Dysb RNAi. Tissues were labeled with anti αRepo antibody to visualize glial cells. Scale bar 20 μm. On the right TEM images of third instar larvae brain showing the Golgi apparatus of ventral ganglion for the above genotypes. Flies expressing UAS-RNAi Dybs ubiquitously showed swelling of largely inflated Golgi cisternae (arrows). Scale bar 500 nm.

Dys1A is reduced in the caudate of schizophrenia cases

Finally, to verify if Dys1A-modulation of basal ganglia-related phenotypes has clinical relevance, we measured Dys1 isoforms in the caudate of schizophrenia cases and matched healthy controls (Supplementary Fig. S6). This revealed reduced Dys1A, but not Dys1C, in patients with schizophrenia compared with controls (Fig. 6a). Notably, previous findings reported reduced Dys1C, but not Dys1A, in the PFC of patients with schizophrenia (17). To directly compare our results to these previous reports, we calculated a mean case control ratio where zero indicates no differences between cases and controls, negative values reduced expression in schizophrenia, and positive values increased expression. In the caudate, Dys1A was reduced in 15 out of 22 case-control pairs, while Dys1C ratios were inconsistent in direction, and of generally smaller magnitude (Fig. 6b). Together, these data suggest that, in contrast to PFC, Dys1A may have a role in basal ganglia-related schizophrenia pathobiology.

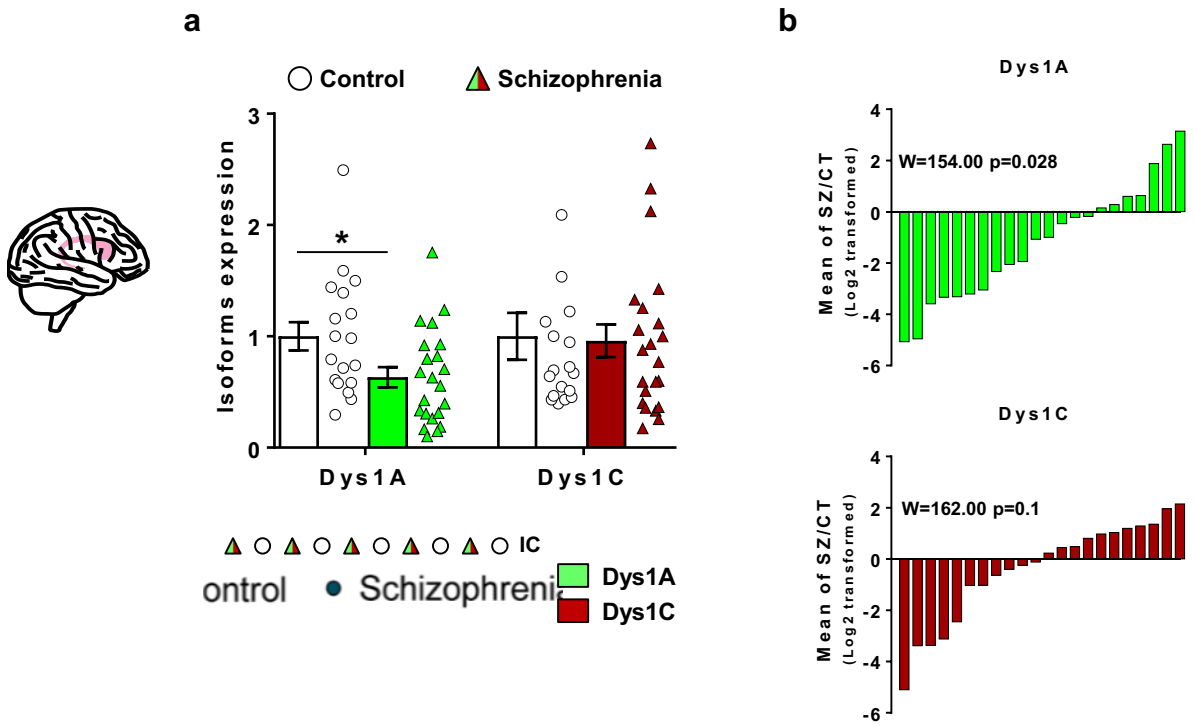

Figure 6. Dys1A, but not Dys1C, is reduced in the caudate of patients with schizophrenia. a. Expression of Dys1A and Dys1C isoforms in postmortem caudate from 22 patients with schizophrenia (Schizophrenia) and 18 matched healthy subjects (Control). No differences were present in non-diagnostic variables (i.e., age, sex, post-mortem interval, pH: Supplementary Fig. S6). Expression of Dys1A, normalized by β-actin, is reduced in the caudate of patients with schizophrenia compared to control subjects (t-test: p=0.02). Dys1C expression is not changed between the two groups (t-test: p=0.71). *p<0.05 vs Control. **b.** Plotting of β-actin normalized data for Dys1A and Dys1C for all case-control pairs. Each bar indicates the log2 transformed ratio of isoform in a schizophrenia case compared to that in its matched control (i.e. the ratio for one case-control pair). Pair-wise analysis of these ratios (Wilcoxon signed-rank test) showed significant difference between schizophrenia cases and their matched controls for Dys1A (W=154.00; p=0.02), but not for Dys1C (W=162.00; p=1.00). Bar graphs show mean ± s.e.m.

Discussion

In this study, we reveal Dys1A as a molecule participating in astrocytic functioning with a bias towards basal ganglia-related behavioral and dopaminergic phenotypes, with implications for schizophrenia. Specifically, the Dys1A isoform that is reduced in the caudate of patients with schizophrenia, is the only Dys1 isoform expressed by astrocytes. Disruption of Dys1A is sufficient to alter astrocytic, but not neuronal, vesicular trafficking and is associated with basal ganglia-dependent, but not PFC-dependent, dopamine and behavioral phenotypes.

Dys1A affected basal ganglia dopaminergic and behavioral functions, while sparing cortex-related phenotypes. In contrast to Dys1A, the expression of Dys1C increases during cortical development (Fig. 2), and it is selectively reduced in PFC of patients with schizophrenia (14). This suggests that well-established Dys1-dependent dopaminergic and behavioral alterations at the cortical level (1, 3, 13, 58) may be more related to neuronal Dys1C. Moreover, recent evidence suggests that astrocytic mechanisms related to dopamine signaling might differ between PFC (21), basal ganglia GPe (20), and NAcc (22). In particular, in the PFC the astroglial vesicular monoamine transporter 2 (VMAT2) has a major involvement on dopaminergic signaling (21), while D2 but not D1 receptors within the GPe (20), and D1 but not D2 receptors in the NAcc (22). Thus, Dys1A modulation of astrocytic functioning and D2 receptor expression may constitute another biological substrate explaining its bias toward basal ganglia dopamine and behavioral alterations. Our findings also suggest astrocytes as a novel player in the dopaminergic cortical/basal ganglia dichotomy and related behavioral abnormalities consistently reported in schizophrenia (59, 60). The differential control exerted by astrocytic Dys1A on cortical and basal ganglia dopamine-related behaviors also adds to increasing evidence for heterogeneous astrocyte-mediated processes across different brain regions (61-63). Future studies are needed to clarify the mechanisms by which astrocytic Dys1A modulates behaviors and related dopaminergic circuits within the basal ganglia.

We reveal that the interaction between astrocytes and dopamine system at the level of the basal ganglia have evident effects on motivated behavior and saliency detection. In particular, Dys1A reduction decreased dopamine content and increased levels of D2 receptors in basal ganglia, and this was associated with avolition and sensorimotor gating deficits. This is in agreement with compelling evidence that dopamine levels in basal ganglia are proportionally related to motivational behavior (64). Similarly, striatal overexpression of D2 receptors by the CaMKII promoter (65), which is also present in astrocytes (66), reduced motivation (49). In contrast, Dys1A disruption affected less gross motor functions and did not alter locomotor responses to amphetamine, despite altering dopamine signaling within GPe. Historically, GPe has been implicated in movement control (67). However, in agreement with our findings, recent studies show GPe involvement in motivational and sensorimotor gating processes (68-71). Moreover, dopaminergic manipulations within GPe may not alter motor functions (68, 71, 72), and D2 receptors do not contribute to amphetamine-evoked astrocytic and locomotor responses (22). Instead, astrocyte-dopamine interactions within VTA-NAcc dopamine/D1 pathways are involved in locomotor processes (22). Overall, our data show that Dys1A regulates astrocytes, motivational and sensorimotor gating processes involving dopamine/D2-dependent alterations in STR/GPe pathways. Astrocytic Dys1A represents therefore a potential cell-specific target for the treatment of motivational and other neuropsychiatric disorders associated with disrupted dopamine/D2 signaling.

In agreement with previous studies on Dys1 (16, 52, 53), we here report that Dys1A reduction is sufficient to disrupt intracellular vesicular trafficking. Dys1-dependent disruptions of vesicular trafficking cause an increased presence on the neuronal surface of those receptors that normally rely on internalization/degradation processes (16, 52, 53). In particular, dopamine D2-like receptors, in contrast to D1-like, follow these intracellular pathways (73, 74), and are consequently influenced by Dys1 disruption (3, 16, 53). Accordingly, we found that Dys1A disruption altered the surface expression of D2 receptors. However, as Dys1A seemed to alter intracellular trafficking mainly in astrocytes and not in neurons, it is tempting to speculate that D2 overexpression would be present only on the

surface of astrocytes. The conundrum would be why Dys1A, which is also expressed in neurons, is influencing primarily astrocytes. It is noteworthy that our developmental profiling reveals that in adult brains, expression of Dys1A is lower than Dys1C. Moreover, we found that in neurons expression of Dys1C is higher than Dys1A. Thus, Dys1A might have a more marginal function in adult neuronal cells. Furthermore, the greater neuronal prominence of Dys1C might compensate the Dys1A disruption. In contrast, as astrocytes express only the Dys1A isoform, its disruption would generate more consistent alterations. In particular, the defective morphology of Golgi apparatus, observed at both structural and molecular level, likely contributes to the impaired secretory traffic or simply reflect altered astrocytic homeostasis dependent specifically from Dys1A disruption. Moreover, the intracellular trafficking markers addressed in our study have been reported to participate in astrocytic functioning and, more importantly, in the regulation of intracellular Ca^{2+} in these cells (75-77). This might then be related to Dys1-dependent alterations astrocytic Ca^{2+} signal dynamics that we observed. Overall, our findings indicate a direct link between Dys1A and astrocyte-related dopaminergic signaling, with an impact on clinically relevant behavioral abnormalities. However, more focused *in vitro* cellular studies are needed to elucidate the exact intracellular mechanisms linking Dys1A and astrocytic functioning.

In summary, we uncovered a previously unexplored role for the Dys1A isoform in the modulation of astrocytic activity and dopamine/D2 signaling that is prevalently evident in basal ganglia, with implications for motivational and sensorimotor gating abilities relevant to schizophrenia. These findings further indicate an astrocyte involvement in dopamine-related behavioral dysfunctions in psychiatric disorders. Indeed, our clinically-relevant findings point to basal ganglia astrocytes as a promising target for the treatment of dopamine dysfunctions in schizophrenia.

Acknowledgments

We thank M. Morini, E. Albanesi, D. Cantatore, G. Pruzzo, T. Catelani, D. Mauro, S. Monari, F. Torri, B. Chiarenza, A. Monteforte and C. Chiabrera, for technical support. We thank GlaxoSmithKline and Dr. S. Wilson for generously donating the newly generated Dys1Aflox mice. We thank Dr. D.R. Weinberger and Dr. R.E. Straub for initial access to the Brain Cloud databank. We thank Dr. L. Tian and Dr. T. Patriarchi for generously sharing the initial dLight virus samples. This work was supported by funding from the Marie Sklodowska-Curie Fellowships (grant n.796244) to CD; the Ministero dell'Universita' e della Ricerca italiano (project PRIN 2017K2NEF4) to FD; grant MIUR Progetto eccellenza to FF; the Istituto Italiano di Tecnologia, the Brain and Behavior Research Foundation (2015 NARSAD grant n.23234), the Ministero della Salute italiano (project GR-2016-02362413), and Fondazione Telethon Italia (project GGP19103) to FP.

Author Contributions

Conceptualization, RM, GT, FM and FP; Methodology and Investigation, RM, GT, DD, CD, GL, AL, LC, FF, VF, GO, RM, FM, GP, AF, GC, MADL, FM and FP; Resources, GO, DR, JLW, GML, GC, CSW, FM and FP; Writing, all authors; Visualization, RM, GT, DD, CD, GL, AL, GL, GO, RM, FM and FP; Supervision, FM and FP; Funding Acquisition, FD, CSW, and FP.

Competing Interests statement

The authors declare no competing interests.

References

1. Leggio GM, Torrisi SA, Mastrogiacomo R, Mauro D, Chisari M, Devroye C, et al. (2019): The epistatic interaction between the dopamine D3 receptor and dysbindin-1 modulates higher-order cognitive functions in mice and humans. *Mol Psychiatry*.
2. Savage JE, Jansen PR, Stringer S, Watanabe K, Bryois J, de Leeuw CA, et al. (2018): Genome-wide association meta-analysis in 269,867 individuals identifies new genetic and functional links to intelligence. *Nat Genet*. 50:912-919.
3. Scheggia D, Mastrogiacomo R, Mereu M, Sannino S, Straub RE, Armando M, et al. (2018): Variations in Dysbindin-1 are associated with cognitive response to antipsychotic drug treatment. *Nat Commun*. 9:2265.
4. Waddington JL, Zhen X, O'Tuathaigh CMP (2019): Developmental Genes and Regulatory Proteins, Domains of Cognitive Impairment in Schizophrenia Spectrum Psychosis and Implications for Antipsychotic Drug Discovery: The Example of Dysbindin-1 Isoforms and Beyond. *Front Pharmacol*. 10:1638.
5. Straub RE, MacLean CJ, O'Neill FA, Burke J, Murphy B, Duke F, et al. (1995): A potential vulnerability locus for schizophrenia on chromosome 6p24-22: evidence for genetic heterogeneity. *Nat Genet*. 11:287-293.
6. Marshall CR, Howrigan DP, Merico D, Thiruvahindrapuram B, Wu W, Greer DS, et al. (2017): Contribution of copy number variants to schizophrenia from a genome-wide study of 41,321 subjects. *Nat Genet*. 49:27-35.
7. Pae CU, Drago A, Kim JJ, Patkar AA, Jun TY, Lee C, et al. (2008): DTNBP1 haplotype influences baseline assessment scores of schizophrenic in-patients. *Neurosci Lett*. 440:150-154.
8. Bray NJ, Preece A, Williams NM, Moskvina V, Buckland PR, Owen MJ, et al. (2005): Haplotypes at the dystrobrevin binding protein 1 (DTNBP1) gene locus mediate risk for schizophrenia through reduced DTNBP1 expression. *Hum Mol Genet*. 14:1947-1954.
9. Straub RE, Jiang Y, MacLean CJ, Ma Y, Webb BT, Myakishev MV, et al. (2002): Genetic variation in the 6p22.3 gene DTNBP1, the human ortholog of the mouse dysbindin gene, is associated with schizophrenia. *American journal of human genetics*. 71:337-348.
10. Voisey J, Swagell CD, Hughes IP, Lawford BR, Young RM, Morris CP (2010): Analysis of HapMap tag-SNPs in dysbindin (DTNBP1) reveals evidence of consistent association with schizophrenia. *Eur Psychiatry*. 25:314-319.
11. Talbot K, Eidem WL, Tinsley CL, Benson MA, Thompson EW, Smith RJ, et al. (2004): Dysbindin-1 is reduced in intrinsic, glutamatergic terminals of the hippocampal formation in schizophrenia. *J Clin Invest*. 113:1353-1363.
12. Weickert CS, Straub RE, McClintock BW, Matsumoto M, Hashimoto R, Hyde TM, et al. (2004): Human dysbindin (DTNBP1) gene expression in normal brain and in schizophrenic prefrontal cortex and midbrain. *Archives of general psychiatry*. 61:544-555.
13. Papaleo F, Weinberger DR (2011): Dysbindin and Schizophrenia: it's dopamine and glutamate all over again. *Biological psychiatry*. 69:2-4.
14. Tang J, LeGros RP, Louneva N, Yeh L, Cohen JW, Hahn CG, et al. (2009): Dysbindin-1 in dorsolateral prefrontal cortex of schizophrenia cases is reduced in an isoform-specific manner unrelated to dysbindin-1 mRNA expression. *Hum Mol Genet*. 18:3851-3863.
15. Wentzel C, Delvendahl I, Sydlik S, Georgiev O, Muller M (2018): Dysbindin links presynaptic proteasome function to homeostatic recruitment of low release probability vesicles. *Nat Commun*. 9:267.
16. Ji Y, Yang F, Papaleo F, Wang HX, Gao WJ, Weinberger DR, et al. (2009): Role of dysbindin in dopamine receptor trafficking and cortical GABA function. *Proceedings of the National Academy of Sciences of the United States of America*. 106:19593-19598.
17. Talbot K, Ong WY, Blake DJ, Tang J, Louneva N, Carlson GC, et al. (2009): Dysbindin-1 and Its Protein Family. In: Javitt DC, Kantrowitz J, editors. *Handbook of Neurochemistry and Molecular Neurobiology*, 3rd ed. New York: Springer Science, pp 107-241.

18. Shao L, Shuai Y, Wang J, Feng S, Lu B, Li Z, et al. (2011): Schizophrenia susceptibility gene dysbindin regulates glutamatergic and dopaminergic functions via distinctive mechanisms in Drosophila. *Proceedings of the National Academy of Sciences of the United States of America*. 108:18831-18836.
19. Shao W, Zhang SZ, Tang M, Zhang XH, Zhou Z, Yin YQ, et al. (2013): Suppression of neuroinflammation by astrocytic dopamine D2 receptors via alphaB-crystallin. *Nature*. 494:90-94.
20. Cui Q, Pitt JE, Pamukcu A, Poulin JF, Mabrouk OS, Fiske MP, et al. (2016): Blunted mGluR Activation Disinhibits Striatopallidal Transmission in Parkinsonian Mice. *Cell Rep*. 17:2431-2444.
21. Petrelli F, Dallerac G, Pucci L, Cali C, Zehnder T, Sultan S, et al. (2018): Dysfunction of homeostatic control of dopamine by astrocytes in the developing prefrontal cortex leads to cognitive impairments. *Mol Psychiatry*.
22. Corkrum M, Covelo A, Lines J, Bellocchio L, Pisansky M, Loke K, et al. (2020): Dopamine-Evoked Synaptic Regulation in the Nucleus Accumbens Requires Astrocyte Activity. *Neuron*.
23. Talbot K, Louneva N, Cohen JW, Kazi H, Blake DJ, Arnold SE (2011): Synaptic dysbindin-1 reductions in schizophrenia occur in an isoform-specific manner indicating their subsynaptic location. *PLoS One*. 6:e16886.
24. Larimore J, Zlatic SA, Gokhale A, Tornieri K, Singleton KS, Mullin AP, et al. (2014): Mutations in the BLOC-1 subunits dysbindin and muted generate divergent and dosage-dependent phenotypes. *The Journal of biological chemistry*. 289:14291-14300.
25. Yuan Y, Wang H, Wei Z, Li W (2015): Impaired autophagy in hilar mossy cells of the dentate gyrus and its implication in schizophrenia. *J Genet Genomics*. 42:1-8.
26. Petit EI, Michalak Z, Cox R, O'Tuathaigh CM, Clarke N, Tighe O, et al. (2017): Dysregulation of Specialized Delay/Interference-Dependent Working Memory Following Loss of Dysbindin-1A in Schizophrenia-Related Phenotypes. *Neuropsychopharmacology*. 42:1349-1360.
27. Huang H, Michetti C, Busnelli M, Manago F, Sannino S, Scheggia D, et al. (2014): Chronic and acute intranasal oxytocin produce divergent social effects in mice. *Neuropsychopharmacology*. 39:1102-1114.
28. Scheggia D, Bebensee A, Weinberger DR, Papaleo F (2014): The ultimate intra-/extra-dimensional attentional set-shifting task for mice. *Biological psychiatry*. 75:660-670.
29. Manago F, Mereu M, Mastwal S, Mastrogiacomo R, Scheggia D, Emanuele M, et al. (2016): Genetic Disruption of Arc/Arg3.1 in Mice Causes Alterations in Dopamine and Neurobehavioral Phenotypes Related to Schizophrenia. *Cell Rep*. 16:2116-2128.
30. Papaleo F, Kieffer BL, Tabarin A, Contarino A (2007): Decreased motivation to eat in mu-opioid receptor-deficient mice. *The European journal of neuroscience*. 25:3398-3405.
31. Polishchuk RS, Mironov AA (2001): Correlative video light/electron microscopy. *Curr Protoc Cell Biol*. Chapter 4:Unit 4 8.
32. Caffino L, Verheij MMM, Roversi K, Targa G, Mottarlini F, Popik P, et al. (2020): Hypersensitivity to amphetamine's psychomotor and reinforcing effects in serotonin transporter knockout rats: Glutamate in the nucleus accumbens. *Br J Pharmacol*. 177:4532-4547.
33. Paxinos G, Franklin KBJ (2004): *The mouse brain in stereotaxic coordinates*. Amsterdam: Elsevier Academic Press.
34. Dugue GP, Dumoulin A, Triller A, Dieudonne S (2005): Target-dependent use of co-released inhibitory transmitters at central synapses. *J Neurosci*. 25:6490-6498.
35. Srinivasan R, Huang BS, Venugopal S, Johnston AD, Chai H, Zeng H, et al. (2015): Ca(2+) signaling in astrocytes from Ip3r2(-/-) mice in brain slices and during startle responses in vivo. *Nature neuroscience*. 18:708-717.
36. Mariotti L, Losi G, Lia A, Melone M, Chiavegato A, Gomez-Gonzalo M, et al. (2018): Interneuron-specific signaling evokes distinctive somatostatin-mediated responses in adult cortical astrocytes. *Nat Commun*. 9:82.
37. Napoli B, Gumeni S, Forgiarini A, Fantin M, De Filippis C, Panzeri E, et al. (2019): Naringenin Ameliorates Drosophila ReepA Hereditary Spastic Paraplegia-Linked Phenotypes. *Front Neurosci*. 13:1202.
38. Orso G, Pendin D, Liu S, Tosetto J, Moss TJ, Faust JE, et al. (2009): Homotypic fusion of ER membranes requires the dynamin-like GTPase atlastin. *Nature*. 460:978-983.

936 39. Scheggia D, Manago F, Maltese F, Bruni S, Nigro M, Dautan D, et al. (2020): Somatostatin
937 interneurons in the prefrontal cortex control affective state discrimination in mice. *Nature neuroscience*.
938 23:47-60.
939 40. Ferretti V, Maltese F, Contarini G, Nigro M, Bonavia A, Huang H, et al. (2019): Oxytocin Signaling in
940 the Central Amygdala Modulates Emotion Discrimination in Mice. *Curr Biol*. 29:1938-1953 e1936.
941 41. Papaleo F, Yang F, Garcia S, Chen J, Lu B, Crawley JN, et al. (2012): Dysbindin-1 modulates prefrontal
942 cortical activity and schizophrenia-like behaviors via dopamine/D2 pathways. *Mol Psychiatry*. 17:85-98.
943 42. Feng YQ, Zhou ZY, He X, Wang H, Guo XL, Hao CJ, et al. (2008): Dysbindin deficiency in sandy mice
944 causes reduction of snapin and displays behaviors related to schizophrenia. *Schizophrenia research*. 106:218-
945 228.
946 43. Hattori S, Murotani T, Matsuzaki S, Ishizuka T, Kumamoto N, Takeda M, et al. (2008): Behavioral
947 abnormalities and dopamine reductions in sdy mutant mice with a deletion in Dtnbp1, a susceptibility gene
948 for schizophrenia. *Biochem Biophys Res Commun*. 373:298-302.
949 44. Robbins TW (2007): Shifting and stopping: fronto-striatal substrates, neurochemical modulation and
950 clinical implications. *Philosophical transactions of the Royal Society of London*. 362:917-932.
951 45. Clarke HF, Hill GJ, Robbins TW, Roberts AC (2011): Dopamine, but not serotonin, regulates reversal
952 learning in the marmoset caudate nucleus. *J Neurosci*. 31:4290-4297.
953 46. Doherty JM, Masten VL, Powell SB, Ralph RJ, Klamer D, Low MJ, et al. (2008): Contributions of
954 dopamine D1, D2, and D3 receptor subtypes to the disruptive effects of cocaine on prepulse inhibition in
955 mice. *Neuropsychopharmacology*. 33:2648-2656.
956 47. Koch M (1999): The neurobiology of startle. *Prog Neurobiol*. 59:107-128.
957 48. Plappert CF, Pilz PK, Schnitzler HU (2004): Factors governing prepulse inhibition and prepulse
958 facilitation of the acoustic startle response in mice. *Behavioural brain research*. 152:403-412.
959 49. Drew MR, Simpson EH, Kellendonk C, Herzberg WG, Lipatova O, Fairhurst S, et al. (2007): Transient
960 overexpression of striatal D2 receptors impairs operant motivation and interval timing. *J Neurosci*. 27:7731-
961 7739.
962 50. Ward RD, Kellendonk C, Kandel ER, Balsam PD (2011): Timing as a window on cognition in
963 schizophrenia. *Neuropharmacology*.
964 51. Ward RD, Kellendonk C, Simpson EH, Lipatova O, Drew MR, Fairhurst S, et al. (2009): Impaired timing
965 precision produced by striatal D2 receptor overexpression is mediated by cognitive and motivational deficits.
966 *Behavioral neuroscience*. 123:720-730.
967 52. Marley A, von Zastrow M (2010): Dysbindin promotes the post-endocytic sorting of G protein-
968 coupled receptors to lysosomes. *PLoS One*. 5:e9325.
969 53. Leggio GM, Torrisi SA, Mastrogiacomo R, Mauro D, Chisari M, Devroye C, et al. (2021): The epistatic
970 interaction between the dopamine D3 receptor and dysbindin-1 modulates higher-order cognitive functions
971 in mice and humans. *Mol Psychiatry*. 26:1272-1285.
972 54. Bucci C, Parton RG, Mather IH, Stunnenberg H, Simons K, Hoflack B, et al. (1992): The small GTPase
973 rab5 functions as a regulatory factor in the early endocytic pathway. *Cell*. 70:715-728.
974 55. Soldati T, Rancano C, Geissler H, Pfeffer SR (1995): Rab7 and Rab9 are recruited onto late endosomes
975 by biochemically distinguishable processes. *The Journal of biological chemistry*. 270:25541-25548.
976 56. Liu X, Cheng C, Shao B, Wu X, Ji Y, Lu X, et al. (2012): The functional interaction between CDK11p58
977 and beta-1,4-galactosyltransferase I involved in astrocyte activation caused by lipopolysaccharide.
978 *Inflammation*. 35:1365-1377.
979 57. Nakamura N, Rabouille C, Watson R, Nilsson T, Hui N, Slusarewicz P, et al. (1995): Characterization of
980 a cis-Golgi matrix protein, GM130. *J Cell Biol*. 131:1715-1726.
981 58. Papaleo F, Burdick MC, Callicott JH, Weinberger DR (2014): Epistatic interaction between COMT and
982 DTNBP1 modulates prefrontal function in mice and in humans. *Mol Psychiatry*. 19:311-316.
983 59. Weinstein JJ, Chohan MO, Slifstein M, Kegeles LS, Moore H, Abi-Dargham A (2017): Pathway-Specific
984 Dopamine Abnormalities in Schizophrenia. *Biological psychiatry*. 81:31-42.
985 60. Winterer G, Weinberger DR (2004): Genes, dopamine and cortical signal-to-noise ratio in
986 schizophrenia. *Trends in neurosciences*. 27:683-690.

61. Chai H, Diaz-Castro B, Shigetomi E, Monte E, Octeau JC, Yu X, et al. (2017): Neural Circuit-Specialized Astrocytes: Transcriptomic, Proteomic, Morphological, and Functional Evidence. *Neuron*. 95:531-549 e539.
62. Ben Haim L, Rowitch DH (2017): Functional diversity of astrocytes in neural circuit regulation. *Nat Rev Neurosci*. 18:31-41.
63. Huang AY, Woo J, Sardar D, Lozzi B, Bosquez Huerta NA, Lin CJ, et al. (2020): Region-Specific Transcriptional Control of Astrocyte Function Oversees Local Circuit Activities. *Neuron*. 106:992-1008 e1009.
64. Mohebi A, Pettibone JR, Hamid AA, Wong JT, Vinson LT, Patriarchi T, et al. (2019): Dissociable dopamine dynamics for learning and motivation. *Nature*. 570:65-70.
65. Simpson EH, Kellendonk C (2017): Insights About Striatal Circuit Function and Schizophrenia From a Mouse Model of Dopamine D2 Receptor Upregulation. *Biological psychiatry*. 81:21-30.
66. Takeuchi Y, Yamamoto H, Fukunaga K, Miyakawa T, Miyamoto E (2000): Identification of the isoforms of Ca(2+)/Calmodulin-dependent protein kinase II in rat astrocytes and their subcellular localization. *J Neurochem*. 74:2557-2567.
67. Gittis AH, Berke JD, Bevan MD, Chan CS, Mallet N, Morrow MM, et al. (2014): New roles for the external globus pallidus in basal ganglia circuits and behavior. *J Neurosci*. 34:15178-15183.
68. Carvalho Poyraz F, Holzner E, Bailey MR, Meszaros J, Kenney L, Kheirbek MA, et al. (2016): Decreasing Striatopallidal Pathway Function Enhances Motivation by Energizing the Initiation of Goal-Directed Action. *J Neurosci*. 36:5988-6001.
69. Fiore VG, Nolte T, Rigoli F, Smittenaar P, Gu X, Dolan RJ (2018): Value encoding in the globus pallidus: fMRI reveals an interaction effect between reward and dopamine drive. *Neuroimage*. 173:249-257.
70. Miller JM, Vorel SR, Tranguch AJ, Kenny ET, Mazzoni P, van Gorp WG, et al. (2006): Anhedonia after a selective bilateral lesion of the globus pallidus. *The American journal of psychiatry*. 163:786-788.
71. Sotoyama H, Zheng Y, Iwakura Y, Mizuno M, Aizawa M, Shcherbakova K, et al. (2011): Pallidal hyperdopaminergic innervation underlying D2 receptor-dependent behavioral deficits in the schizophrenia animal model established by EGF. *PLoS One*. 6:e25831.
72. Avila G, Picazo O, Chuc-Meza E, Garcia-Ramirez M (2020): Reduction of dopaminergic transmission in the globus pallidus increases anxiety-like behavior without altering motor activity. *Behavioural brain research*. 386:112589.
73. Bartlett SE, Enquist J, Hopf FW, Lee JH, Gladher F, Kharazia V, et al. (2005): Dopamine responsiveness is regulated by targeted sorting of D2 receptors. *Proceedings of the National Academy of Sciences of the United States of America*. 102:11521-11526.
74. Thompson D, Whistler JL (2011): Dopamine D(3) receptors are down-regulated following heterologous endocytosis by a specific interaction with G protein-coupled receptor-associated sorting protein-1. *The Journal of biological chemistry*. 286:1598-1608.
75. Jiang M, Chen G (2009): Ca2+ regulation of dynamin-independent endocytosis in cortical astrocytes. *J Neurosci*. 29:8063-8074.
76. Boulay AC, Saubamea B, Adam N, Chasseigneaux S, Mazare N, Gilbert A, et al. (2017): Translation in astrocyte distal processes sets molecular heterogeneity at the gliovascular interface. *Cell Discov*. 3:17005.
77. Xin H, Wang F, Li Y, Lu QE, Cheung WL, Zhang Y, et al. (2017): Secondary Release of Exosomes From Astrocytes Contributes to the Increase in Neural Plasticity and Improvement of Functional Recovery After Stroke in Rats Treated With Exosomes Harvested From MicroRNA 133b-Overexpressing Multipotent Mesenchymal Stromal Cells. *Cell Transplant*. 26:243-257.